Iron-deplete diet enhances *Caenorhabditis elegans* lifespan via oxidative stress response pathways

Priyanka Das[1], Ravi[1], and Jogender Singh[1,*]

[1]Department of Biological Sciences, Indian Institute of Science Education and Research, Mohali, Punjab, 140306, India

[*]For correspondence: jogender@iisermohali.ac.in

Keywords: iron; lifespan; oxidative stress; HLH-30; SKN-1

Abstract

Gut microbes play a crucial role in modulating host lifespan. However, the microbial factors that influence host longevity and their mechanisms of action remain poorly understood. Using the expression of *Caenorhabditis elegans* FAT-7, a stearoyl-CoA 9-desaturase, as a proxy for lifespan modulation, we conduct a genome-wide bacterial mutant screen and identify 26 *Escherichia coli* mutants that enhance host lifespan. Transcriptomic and biochemical analyses reveal that these mutant diets induce oxidative stress and activate the mitochondrial unfolded protein response (UPRmt). Lifespan extension requires the oxidative stress response regulators SKN-1, SEK-1, and HLH-30. Mechanistically, these effects are linked to reduced iron availability, as iron supplementation restores FAT-7 expression, suppresses UPRmt activation, and abolishes lifespan extension. Iron chelation mimics the pro-longevity effects of the mutant diets, highlighting dietary iron as a key modulator of aging. Our findings reveal a bacterial-host metabolic axis that links iron homeostasis, oxidative stress, and longevity in *C. elegans*.

Introduction

Aging is a pathophysiological process characterized by the gradual decline of cellular and tissue functions, which significantly increases the risk of age-related disorders, including neurodegenerative diseases, cardiovascular diseases, type 2 diabetes, and cancer (Li et al., 2021). However, like many other biological processes, aging is regulated by canonical signaling pathways and transcription factors, making it amenable to modulation through targeted interventions (Kenyon, 2010). According to the geroscience hypothesis, interventions that extend lifespan may also prevent, delay, and mitigate age-associated disorders (Chmielewski et al., 2024; Kennedy et al., 2014; Li et al., 2021; López-Otín et al., 2013). Numerous studies have demonstrated that aging can be modulated through genetic, dietary, and pharmacological approaches (Chmielewski et al., 2024; Masoro, 2005; Selman, 2014; Speakman and Mitchell, 2011). For instance, dietary restriction has been shown to extend lifespan and delay the onset of multiple age-related pathologies across various organisms (Chmielewski et al., 2024; Masoro, 2005; Selman, 2014; Speakman and Mitchell, 2011). While ongoing research continues to explore novel therapeutics for aging regulation, there remains a critical need for interventions that are not only effective but also safe, accessible, and practical for everyday implementation.

The gut microbiota, comprising all microorganisms residing in the gastrointestinal tract of an organism, plays a crucial role in maintaining host health and lifespan (Debnath et al., 2021; Rooks and Garrett, 2016; Wang et al., 2024). Its composition changes progressively with age, suggesting that microbiota dysbiosis may represent an additional hallmark of aging (Biagi et al., 2017; Molinero et al., 2023). Indeed, several studies have linked microbial dysbiosis to aging and age-related pathologies (Ragonnaud and Biragyn, 2021). Microbiome-based treatments hold promise due to their potential to modify gut microbe composition through oral interventions (Smith et al., 2017). Moreover, identifying age-modulating metabolites from the microbiome could yield novel strategies for combating aging-related disorders (Gong et al., 2023; Shi et al., 2024).

The nematode *Caenorhabditis elegans* is a widely used model organism in aging research (Kenyon, 2010; Mack et al., 2018). As a bacterivore, *C. elegans* thrives on various bacterial diets, and bacterial metabolites have been shown to influence key life-history traits, including lifespan, making it an excellent system for studying gut microbe-host interactions in aging (M. Feng et al., 2023; Zhang et al., 2017). To date, four distinct genome-wide

Escherichia coli screens have been conducted to identify bacterial mutants that enhance *C. elegans* lifespan (B. Han et al., 2017; Khanna et al., 2016; Shin et al., 2020; Virk et al., 2016). These screens have identified bacterial mutants and metabolites that promote longevity through diverse mechanisms, including dauer formation, activation of the mitochondrial unfolded protein response (UPRmt), and folate limitation (B. Han et al., 2017; Khanna et al., 2016; Shin et al., 2020; Virk et al., 2016). Surprisingly, these screens have yielded only minimal overlap in identified mutants (Figure S1A), possibly due to poor resolution—often limited to a few time-point measurements—and technical variations, such as differences in liquid versus solid nematode growth media. Nonetheless, these studies suggest that existing screens are far from saturation and that additional *E. coli* mutants and mechanisms influencing *C. elegans* lifespan remain to be discovered. They also highlight the need for high-resolution primary screens utilizing phenotypes that serve as proxies for lifespan, followed by secondary screens to validate lifespan changes.

Lipid composition, particularly monounsaturated fatty acid (MUFA) levels, is known to influence lifespan (Schroeder and Brunet, 2015). Long-lived *C. elegans* mutants, including those with reduced insulin-like signaling or dietary restriction mimetics, exhibit elevated MUFA levels (Reis et al., 2011). Δ9 desaturases are key lipogenic enzymes that synthesize MUFAs from saturated fatty acids. *C. elegans* encodes three Δ9 desaturases—FAT-5, FAT-6, and FAT-7 (Brock et al., 2007). Among these, FAT-6 and FAT-7 catalyze the conversion of stearic acid to oleic acid. Studies have shown that dietary MUFA supplementation extends *C. elegans* lifespan, and the expression of Δ9 desaturases is closely linked to aging (Brock et al., 2007; Castillo-Quan et al., 2023; S. Han et al., 2017; Reis et al., 2011, 2011; Schroeder and Brunet, 2015). Interestingly, Δ9 desaturase activity is diet-regulated, with diets rich in unsaturated fatty acids repressing their expression (Brock et al., 2007; Choi et al., 1996; Ntambi and Miyazaki, 2003). Given that diet modulates Δ9 desaturase expression and these enzymes are associated with aging, we hypothesized that Δ9 desaturase expression levels could serve as a marker to identify *E. coli* mutants that influence host lifespan.

In this study, we conducted a genome-wide *E. coli* mutant screen to identify microbial factors that modulate *C. elegans* FAT-7 levels. We identified 26 *E. coli* mutants that reduced FAT-7 expression and investigated their effects on host lifespan. Notably, *C. elegans* fed on all 26 *E. coli* mutants exhibited extended lifespan. Transcriptomic analysis of *C. elegans* exposed to these bacterial mutants suggested that the worms experienced oxidative stress on these diets. Additionally, we observed activation of the UPRmt in *C. elegans* fed on the

mutant *E. coli* strains. Further investigation revealed that iron supplementation reversed all observed phenotypes, including FAT-7 expression, UPRmt activation, and lifespan extension. Conversely, dietary iron limitation recapitulated the effects of the mutant *E. coli* diets, inducing UPRmt activation and lifespan extension. Finally, we demonstrated that the increased lifespan observed under iron-depleted conditions was mediated by genetic pathways associated with oxidative stress responses, including the nuclear factor erythroid 2-related factor SKN-1, the MAP kinase kinase SEK-1, and the TFEB ortholog HLH-30. Our findings uncover a metabolic interaction between bacteria and the host that connects iron homeostasis, oxidative stress, and longevity in *C. elegans*.

Results

Genome-wide bacterial screen identifies *E. coli* mutants that modulate *C. elegans* FAT-7 levels

To identify *E. coli* mutants that enhance the lifespan of *C. elegans*, we used changes in *C. elegans* FAT-7 expression as a proxy for lifespan alterations. We designed a genome-wide screen using the Keio collection to identify *E. coli* mutants that modify *C. elegans* FAT-7 expression, utilizing the *fat-7p::fat-7::GFP* reporter strain. Mutants that alter FAT-7 expression would subsequently be tested for their effects on *C. elegans* lifespan in a secondary screen (Figure 1A). The Keio collection consists of single-gene deletion mutants in 3,985 genes of the *E. coli* BW25113 strain (Baba et al., 2006). Synchronized L1 larvae of the FAT-7 reporter strain were fed individual *E. coli* mutants seeded on nematode growth medium (NGM) plates and allowed to develop into gravid adults. Plates were then screened under a fluorescence stereomicroscope to identify mutants that caused either an increase or decrease in green fluorescence protein (GFP) expression compared to the wild-type *E. coli* BW25113 strain (Figure 1A).

From this primary screen, we identified 26 *E. coli* mutants that significantly reduced FAT-7::GFP levels (Figure 1B, Figure S1B, Table S1). However, no mutants were found that significantly increased FAT-7::GFP expression. For clarity, we will refer to the *E. coli* mutants that suppressed FAT-7 expression in *C. elegans* as mutant diets, while the BW25113 strain will be referred to as the control diet. Notably, worms fed on all the mutant diets exhibited delayed development compared to those grown on the control diet (Figure 1C).

Gene ontology (GO) analysis for the molecular function of the identified bacterial mutants revealed enrichment of categories related to electron transport and oxidoreductase activity (Figure

S1C). This suggested that the *E. coli* mutants that suppress FAT-7::GFP might have a disrupted redox balance.

E. coli mutants that decrease FAT-7 levels extend *C. elegans* lifespan

Next, we tested whether the *E. coli* mutants that reduce FAT-7 levels also impact the lifespan of *C. elegans*. Notably, all mutant diets increased the mean survival of worms compared to those grown on the control diet (Figure 2A-D, S2). Comparing these hits with *E. coli* mutants identified in previous lifespan-enhancing screens revealed no overlap with earlier findings (Figure S3). These results suggest that FAT-7 expression serves as a reliable proxy for identifying diets that promote longevity.

The identified hits were associated with diverse pathways. To investigate the mechanisms underlying their effects, we selected four mutant diets linked to distinct metabolic processes: Δ*tktA*, Δ*yciA*, Δ*pdeI*, and Δ*allD*. *tktA* encodes the primary transketolase enzyme in *E. coli* that serves as a reversible link between glycolysis and the pentose phosphate pathway. *yciA* encodes an acyl-CoA thioesterase, *pdeI* encodes a predicted c-di-GMP-specific phosphodiesterase, and *allD* encodes ureidoglycolate dehydrogenase, involved in allantoin assimilation. Worms fed these four mutant diets displayed enhanced lifespans compared to those on the control diet (Figure 3A).

FAT-7 converts stearic acid to oleic acid, and elevated oleic acid levels are known to suppress *fat-7* expression (Venkatesh et al., 2023). We hypothesized that diets reducing FAT-7 expression might elevate oleic acid levels in *C. elegans*. Previous studies have shown that oleic acid supplementation extends *C. elegans* lifespan (S. Han et al., 2017), suggesting that lifespan extension on mutant diets might result from increased oleic acid levels. FAT-2 encodes a Δ12 desaturase, and mutants lacking *fat-2* cannot convert oleic acid into linoleic acid, leading to elevated oleic acid levels (Watts and Browse, 2002). To examine whether oleic acid accumulation accounts for the extended lifespan observed with mutant diets, we studied the survival of *fat-2(wa17)* hypomorphic mutants on the four selected diets. Surprisingly, *fat-2(wa17)* animals exhibited an increased lifespan on these diets (Figure 3B), suggesting that the lifespan extension is unlikely to be due to oleic acid accumulation in *C. elegans* fed the mutant diets.

Mutant *E. coli* diets induce oxidative stress in *C. elegans*

To investigate the mechanisms underlying the increased lifespan of *C. elegans* on mutant *E. coli* diets, we examined transcriptomic changes in worms fed these diets. Wild-type worms were grown on the control diet and four mutant diets (*ΔtktA*, *ΔpdeI*, *ΔyciA*, and *ΔallD*) until day-1 adulthood, followed by RNA sequencing. Comparative analysis revealed that 1,281 upregulated genes were shared across worms fed all four mutant diets (Figure 3C, Table S2). Similarly, a significant overlap was observed among downregulated genes (Figure S4A, Table S3). These findings suggested a shared molecular mechanism underlying the lifespan-enhancing effects of these diets.

GO analysis of the molecular functions associated with the downregulated genes on all mutant diets revealed enrichment for nucleic acid binding and protein heterodimerization activities (Figure S4B). On the other hand, GO analysis of the 1,281 genes upregulated on all mutant diets showed enrichment for molecular functions related to monooxygenase, oxidoreductase, UDP-glucosyltransferase, and iron ion binding activities (Figure 3D). Notably, these genes are linked to detoxification pathways and are typically upregulated in response to oxidative stress. This suggested that worms feeding on mutant diets may experience elevated reactive oxygen species (ROS) levels compared to those on the control diet. Measurements of ROS levels confirmed this hypothesis, showing significantly increased ROS levels in worms fed mutant diets compared to the control diet (Figure 3E, F).

Mutant *E. coli* diets that suppress *C. elegans* FAT-7 activate host mitochondrial UPR

Mitochondria are highly sensitive to ROS levels, which can create a proteotoxic environment and disrupt protein trafficking across the inner mitochondrial membrane (Melber and Haynes, 2018). Such disruptions can impair mitochondrial protein import and activate the UPRmt, a conserved pathway that restores mitochondrial homeostasis (Melber and Haynes, 2018; Shpilka and Haynes, 2018). Activation of the UPRmt has been associated with lifespan extension in *C. elegans* (Bennett and Kaeberlein, 2014; Shpilka and Haynes, 2018; Xin et al., 2022).

Our transcriptomic analysis suggested elevated ROS levels in worms fed mutant diets. To determine whether UPRmt was activated in worms fed mutant diets, we examined the expression of *hsp-6*, a mitochondrial chaperone and reporter for UPRmt activation (Yoneda et al., 2004). We grew *hsp-6p::GFP* worms on the mutant diets until the day-1-adult stage. GFP fluorescence levels were significantly increased in worms fed mutant diets compared to the control diet, indicating UPRmt activation (Figure 4A, B).

Next, we investigated whether UPRmt activation is required for the lifespan extension observed on the mutant diets. ATFS-1, a key transcription factor, contains a mitochondrial localization signal and a weak nuclear localization signal. Under normal conditions, ATFS-1 is imported into mitochondria and degraded. However, during mitochondrial dysfunction, its import is blocked, and ATFS-1 translocates to the nucleus to activate the UPRmt (Nargund et al., 2012). We analyzed the survival of the ATFS-1 loss-of-function mutant *atfs-1(gk3094)* on the mutant diets. The lifespan extension observed on the mutant diets was abolished in *atfs-1(gk3094)* animals (Figure 4C). These findings demonstrated that UPRmt activation is essential for the lifespan-enhancing effects of mutant diets in *C. elegans*.

Iron supplementation rescues mutant diet-induced phenotypes

A previous study by Zhang et al. identified *E. coli* Keio mutants that delayed *C. elegans* development (Zhang et al., 2019). Interestingly, most of these mutants also upregulated *hsp-6p::GFP* expression in *C. elegans*. Similarly, our study observed delayed development and increased *hsp-6* expression in worms fed on mutant diets. A comparison between the two studies revealed a nearly complete overlap, with 23 out of 26 mutants from our screen matching those identified by Zhang et al. (Figure S5A). Zhang et al. attributed the observed phenotypes to elevated ROS levels and reduced bioavailable iron in *E. coli* mutants.

Based on these findings, we hypothesized that the phenotypes observed on mutant diets could be due to low bioavailable iron. Indeed, supplementing mutant diets with ferric chloride restored worm development and *hsp-6p::GFP* expression to levels observed on the control diet (Figure 5A-C, S5B). Ferric chloride supplementation also rescued the reduced FAT-7::GFP expression levels to those seen on the control diet (Figure 5D, E). Moreover, the pro-longevity effects of mutant diets were abolished with ferric chloride supplementation (Figure 5F, G). Taken together, these data demonstrated that iron supplementation rescues all phenotypes associated with the mutant diets.

Low dietary iron mimics mutant diet-induced phenotypes

To determine whether low iron levels directly cause the observed phenotypes, we tested the effects of the iron chelator 2,2'-bipyridyl. Worms fed on *E. coli* grown with bipyridyl exhibited delayed development (Figure 6A), increased *hsp-6p::GFP* expression (Figure 6B, C), and

reduced *fat-7::GFP* expression (Figure 6D, E). Importantly, bipyridyl supplementation extended *C. elegans* lifespan (Figure 6F). These findings showed that iron chelation mimics all the effects of the mutant diets.

To explore whether the lifespan extension observed under iron chelation and on mutant diets involved overlapping mechanisms, we studied the survival of worms fed on mutant diets upon supplementation with bipyridyl. While supplementation of bipyridyl enhanced *C. elegans* lifespan on the control diet (Figure 6F), it did not further extend the lifespan on mutant diets (Figure 6G-K). Taken together, these results suggested that the lifespan extension induced by mutant diets arises from a low-iron environment, similar to that created by bipyridyl supplementation.

Lifespan extension under low dietary iron depends on oxidative stress response pathways

We next investigated the host genetic pathways involved in the lifespan extension observed under iron-depleted conditions. Since our screen utilized FAT-7 expression, we tested whether the nuclear hormone receptor NHR-49, which regulates FAT-7 and lifespan (Naim et al., 2021; Ratnappan et al., 2014), was required for lifespan extension. The *nhr-49* loss-of-function mutant exhibited extended lifespan on mutant diets, suggesting that NHR-49 is not essential for lifespan extension (Figure S6A). Because worms experienced oxidative stress on the mutant diets (Figure 3E, F), we asked whether oxidative stress response pathways are required for the increased lifespan. The hypoxia-inducible factor (HIF-1) is activated by ROS and is required for lifespan extension mediated by ROS (Hwang et al., 2014; Lee et al., 2010; Ravi and Singh, 2025). We examined whether HIF-1 was required for increased lifespan on the mutant diets. The *hif-1* loss-of-function mutant exhibited an enhanced lifespan on the mutant diets, indicating that HIF-1 was not required for the increased lifespan (Figure S6B).

Multiple molecular pathways regulate the response to oxidative stress. To investigate their role in extending *C. elegans* lifespan on mutant diets, we examined several key components of oxidative stress response pathways. The nuclear factor erythroid 2-related factor SKN-1 plays important roles in metabolism, aging, and orchestrating defense responses against various ROS molecules (Blackwell et al., 2015; Paek et al., 2012; Turner et al., 2024; Walker et al., 2000). We observed that *skn-1(zj15)* animals did not exhibit lifespan extension on the mutant diets (Figure 7A), indicating that SKN-1 is essential for the increased lifespan observed under these conditions. The MAP kinase kinase SEK-1, which is critical for oxidative stress response and acts upstream

of SKN-1 (Hoeven et al., 2011; Inoue et al., 2005), was likewise necessary for lifespan enhancement, as *sek-1(km4)* mutants did not display extended lifespan on the mutant diets (Figure 7B). Similarly, the TFEB homolog HLH-30, which is activated by multiple stresses, including oxidative stress (Lin et al., 2018), was also required for lifespan extension. The *hlh-30(tm1978)* worms failed to show an extended lifespan on the mutant diets (Figure 7C).

Finally, we tested whether these oxidative stress response pathways were also required for lifespan extension under iron-depleted conditions. To this end, we studied the lifespan of *skn-1(zj15)*, *sek-1(km4)*, and *hlh-30(tm1978)* animals upon iron chelation. Supplementation of bipyridyl did not increase the lifespan of *skn-1(zj15)*, *sek-1(km4)*, and *hlh-30(tm1978)* animals (Figure 7D-F). Together, these findings demonstrated that oxidative stress response pathways, including those involving SKN-1, SEK-1, and HLH-30, are critical for lifespan extension on both mutant diets and iron-depleted conditions.

Discussion

In this study, we identified 26 *E. coli* mutants that extend *C. elegans* lifespan. Our findings represent a distinct set of pro-longevity bacterial mutants compared to those identified in previous genome-wide screens (Figure S3), thereby expanding our understanding of how microbiota influence host lifespan. To identify bacterial mutants that enhance *C. elegans* longevity, we used FAT-7 levels as a screening readout. The relationship between FAT-7 expression and lifespan appears to be complex. Previous studies have shown that increased FAT-7 expression correlates with lifespan extension (S. Han et al., 2017). Conversely, compared to an *E. coli* diet, a *Comamonas aquatica* DA1877 diet reduces both FAT-7 expression and lifespan (Han et al., 2024; MacNeil et al., 2013). In contrast, our study shows that *E. coli* mutants that lower FAT-7 expression enhance *C. elegans* lifespan. However, our findings indicate that FAT-7 levels may not be causally linked to lifespan extension, suggesting the involvement of alternative mechanisms driving the observed longevity effects. Nonetheless, since all 26 *E. coli* mutants that reduced FAT-7 expression also extended *C. elegans* lifespan, FAT-7 expression could serve as a reliable proxy for monitoring lifespan changes.

A previous screen by Zhang et al. identified 244 *E. coli* mutants that delayed *C. elegans* development, with most of these mutants also increasing *hsp-6* expression (Zhang et al., 2019). The *E. coli* mutants identified in our screen exhibited the same phenotypes in *C. elegans* and showed a nearly complete overlap with those identified by Zhang et al. However, our screen

identified far fewer mutants. One possible explanation is that the *fat-7::GFP* strain used in our study has low baseline GFP fluorescence on the control diet, potentially leading to the exclusion of mutant diets that caused only mild reductions in FAT-7 levels. Zhang et al. reported that their identified *E. coli* mutants exhibited high ROS levels, which could lead to iron depletion in *C. elegans*. (Zhang et al., 2019). We found that *C. elegans* fed on our *E. coli* mutants also exhibited elevated ROS levels. Iron supplementation restored all mutant diet-induced phenotypes to control levels, suggesting that iron limitation may underlie these effects. Consistently, iron chelation in control diets recapitulated the same phenotypes observed with mutant diets.

Iron is an essential trace element required for various cellular processes, including oxygen transport, energy metabolism, DNA synthesis, and gene regulation (Wang and Pantopoulos, 2011). Maintaining optimal iron levels is crucial for cellular homeostasis, as both iron deficiency and excess can be detrimental (Galaris et al., 2019; Zhang et al., 2019). Interestingly, both high and low iron levels have been shown to extend *C. elegans* lifespan, possibly through hormetic responses that activate stress-related pathways (Bhat et al., 2024; Schiavi et al., 2015). One potential mechanism by which iron depletion extends lifespan is through reduced ferroptosis, a form of iron-dependent cell death (Jenkins et al., 2020; Kim et al., 2022). Alternatively, iron depletion may disrupt iron-sulfur cluster formation, a process that has been linked to lifespan extension in *C. elegans* (Sheng et al., 2021).

Frataxin, a key protein involved in iron-sulfur cluster biogenesis, has been implicated in lifespan regulation (Ast et al., 2019; Schiavi et al., 2013). Inhibition of frataxin extends *C. elegans* lifespan, potentially by disrupting iron-sulfur cluster formation (Schiavi et al., 2023, 2015). Frataxin silencing promotes longevity through multiple mechanisms, including mitophagy activation, HIF-1 signaling, and ferroptosis inhibition (Schiavi et al., 2023, 2015, 2013). While iron depletion appears to mediate some of the effects of frataxin inhibition, the two processes also involve distinct mechanisms. For instance, frataxin inhibition extends lifespan via HIF-1 activation, whereas iron chelation does so independently of HIF-1 (Schiavi et al., 2015). Similarly, the bacterial mutants identified in our study enhanced lifespan in a HIF-1-independent manner, suggesting that frataxin inhibition may activate additional pathways beyond iron limitation.

We observed that *C. elegans* fed on mutant diets exhibited elevated ROS levels. While increased ROS can promote *C. elegans* longevity (Hwang et al., 2014; Lee et al., 2010; Schulz et al., 2007; Yang and Hekimi, 2010), its effects on lifespan are complex and context-dependent,

involving multiple pathways (Hwang et al., 2014; Schaar et al., 2015; Yang and Hekimi, 2010). For example, depending on the type of ROS involved, HIF-1 may or may not be required for ROS-mediated lifespan extension (Lee et al., 2010; Yang and Hekimi, 2010). Likewise, the role of SKN-1 in ROS-mediated longevity varies depending on the specific context (Hwang et al., 2014; Wei and Kenyon, 2016; Yang and Hekimi, 2010). We found that the oxidative stress response pathways SKN-1, SEK-1, and HLH-30 were essential for lifespan extension on mutant diets and under iron-depleted conditions. SEK-1, a MAPK kinase, is an upstream regulator of SKN-1 (Hoeven et al., 2011; Inoue et al., 2005), suggesting that these two factors may act in the same pathway to regulate lifespan under iron-limited conditions. Although HLH-30 is known to be activated by oxidative stress (Lin et al., 2018), its role in ROS-mediated lifespan extension had not been previously investigated. Our findings suggest that HLH-30 plays a key role in lifespan extension under both high ROS and low iron conditions. It is also possible that additional factors from the *E. coli* mutant diets identified in our study contribute to *C. elegans* lifespan extension. Future research investigating bacterial metabolites from these *E. coli* mutants could provide further insights into how gut microbiota influences host longevity.

Materials and methods

Bacterial strains

The bacterial strains used in this study include *Escherichia coli* OP50, *E. coli* BW25113, and mutants from the *E. coli* Keio collection (Baba et al., 2006). *E. coli* OP50 and *E. coli* BW25113 cultures were grown in Luria-Bertani (LB) broth at 37°C, whereas Keio collection mutants were grown in LB broth supplemented with 25 µg/mL kanamycin at 37°C.

C. elegans strains and growth conditions

C. elegans hermaphrodites were maintained on NGM plates seeded with *E. coli* OP50 at 20°C unless otherwise specified. The Bristol N2 strain was used as the wild-type control unless indicated otherwise. The following strains were used in this study: DMS303 *nIs590* [*fat-7p::fat-7::GFP + lin15*(+)], BX26 *fat-2(wa17)*, SJ4100 *zcIs13* [*hsp-6p::GFP + lin-15(+)*], VC3201 *atfs-1(gk3094)*, QV225 *skn-1(zj15)*, KU4 *sek-1(km4)*, JIN1375 *hlh-30(tm1978)*, STE68 *nhr-49(nr2041)*, and ZG31 *hif-1(ia4)*. Some of the strains were obtained from the Caenorhabditis Genetics Center (University of Minnesota, Minneapolis, MN). For

all the experiments, worms were synchronized by bleach treatment to obtain same-stage L1 larvae.

Preparation of NGM plates with different supplements

The following supplements were obtained from HiMedia BioSciences: ferric chloride (#TC583) and 2,2'-bipyridyl (#GRM791). A 1 M stock solution of ferric chloride was prepared in water, while a 100 mM stock solution of 2,2'-bipyridyl was prepared in dimethyl sulfoxide (DMSO). Both stock solutions were stored at -20°C. and diluted to their final concentrations in NGM before pouring the plates. For the 2,2'-bipyridyl supplement, equivalent amounts of DMSO were added to the control plates.

***E. coli* deletion mutant screening for diets that modulate *C. elegans* FAT-7 levels**

Bacterial mutants were grown overnight at 37°C in LB broth supplemented with 25 µg/mL kanamycin in 96-well plates. Subsequently, 30 µL of the overnight cultures were seeded onto 24-well plates containing NGM agar supplemented with 25 µg/mL kanamycin. The plates were incubated at room temperature for at least two days to allow bacterial growth before use in experiments. For screening, embryos of the *fat-7p::fat-7::GFP* strain were harvested from gravid adults using an alkaline bleach solution and incubated in M9 buffer at room temperature for 22 hours to obtain synchronized L1 larvae. Approximately 30–40 synchronized L1 larvae were transferred to each well of 24-well NGM agar plates seeded with individual *E. coli* single-gene deletion mutants and incubated at 20°C. Since FAT-7 levels vary across developmental stages, screening was performed at the day-1-adult stage to identify mutants that modulate FAT-7 expression. GFP fluorescence was monitored in each well to identify *E. coli* mutants that either enhanced or suppressed FAT-7 levels compared to the *E. coli* BW25113 control diet.

Bacterial mutants identified as hits in the initial screen were retested three times on individual NGM plates seeded with the corresponding mutants. *E. coli* mutants that consistently reproduced the phenotype across three independent trials were considered as primary hits. Gene ontology analysis was performed using the DAVID Bioinformatics Database (https://david.ncifcrf.gov/tools.jsp).

C. elegans longevity assays

Lifespan assays were conducted as described earlier (Das et al., 2024). Briefly, gravid adults were lysed using an alkaline bleach solution to obtain embryos, which were then incubated in M9 buffer for 20–24 hours to synchronize them at the L1 larval stage. Synchronized L1 larvae were transferred to NGM plates seeded with either wild-type *E. coli* BW25113 or bacterial mutants identified from the FAT-7::GFP screen. At the late L4 larval stage, the animals were transferred to corresponding bacterial diet plates supplemented with 50 µg/mL FUdR and incubated at 20°C. Worms were monitored daily or every other day and scored as alive or dead. Animals that failed to exhibit touch-provoked movement were classified as dead, while those that crawled off the plates were censored from the analysis. For the lifespan analysis, young adult animals were designated as day 0. Three independent experiments were performed.

C. elegans development assays

Gravid N2 hermaphrodites were lysed with an alkaline bleach solution to isolate eggs, which were then incubated in M9 buffer at room temperature for 22 hours. Approximately 50–100 synchronized L1 larvae were transferred onto NGM plates seeded with either the *E. coli* BW25113 control or mutant diets and incubated at 20°C for 60 hours. Animals at various developmental stages (L1/L2, L3, L4, and adult) were subsequently quantified. The experiment was repeated in at least three independent biological replicates.

Quantification of reactive oxygen species (ROS) levels

ROS levels were quantified using 2',7'-dichlorofluorescein diacetate (DCFHDA, Sigma-Aldrich #35845). A 50 mM DCFHDA stock was prepared in DMSO and stored at -20˚C. Before each experiment, a 50 µM DCFHDA working solution was freshly prepared in M9 buffer. Synchronized L1 larvae of N2 worms were obtained as described above and grown on the *E. coli* BW25113 control and mutant diets until the day-1 adult stage at 20˚C. Subsequently, 15-20 worms were transferred to 150 µL M9 buffer, followed by the addition of 150 µL of the DCFHDA working solution, resulting in a final DCFHDA concentration of

25 µM. Samples were incubated in the dark at room temperature for 5 hours with gentle shaking. Next, the worms were pelleted, the supernatant was removed, and the worms were washed twice with PBS containing 0.01% triton X-100. The prepared samples were then subjected to fluorescence imaging. The 2',7'-dichlorofluorescein (DCF) fluorescence was visualized using a GFP filter on a fluorescence microscope. At least five worms per condition were imaged, and three independent biological replicates were performed.

Fluorescence imaging

Fluorescence imaging was carried out as described previously (Gokul and Singh, 2022; Ravi et al., 2023). Briefly, animals were anesthetized using M9 buffer containing 50 mM sodium azide and placed on 2% agarose pads. The animals were then visualized using either a Nikon SMZ-1000 or SMZ18 fluorescence stereomicroscope. Quantification of fluorescence intensity was done using ImageJ software.

RNA sequencing and data analysis

Synchronized L1 larvae were obtained from wild-type animals as described above and grown on the *E. coli* BW25113 control diet and four mutant diets, including Δ*tktA*, Δ*pdeI*, Δ*yciA*, and Δ*allD*. Total RNA was extracted from three biological replicates using the RNeasy Plus Universal Kit (Qiagen, the Netherlands). Library preparation and sequencing were performed at Unipath Specialty Laboratory Ltd., India. cDNA libraries were sequenced on the NovaSeq 6000 platform using 150-bp paired-end reads.

RNA sequencing data were processed and analyzed using the Galaxy web platform (https://usegalaxy.org/), as described previously (Ghosh and Singh, 2024; Rao et al., 2024). Paired-end reads were first trimmed using the Trimmomatic tool and aligned to the *C. elegans* genome (WS220) with the STAR aligner. Gene expression levels were quantified using htseq-count, and differential expression analysis was performed using DESeq2. Genes with at least a twofold change and $p < 0.01$ were considered differentially expressed. Gene ontology enrichment analysis was conducted using the DAVID Bioinformatics Database. Venn diagrams were generated using the InteractiVenn tool (Heberle et al., 2015).

Quantification and statistical analysis

Statistical analyses were performed with Prism 8 (GraphPad). All error bars represent the mean ± standard deviation (SD). An unpaired, two-tailed, two-sample *t*-test was used when applicable, with statistical significance set at $p < 0.05$. In the figures, statistical significance is indicated by asterisks: * for $p < 0.05$, ** for $p < 0.01$, and *** for $p < 0.001$, relative to the relevant controls. Survival fractions were calculated using the Kaplan-Meier method, and statistical significance between survival curves was determined using the log-rank test. All experiments were performed in triplicate.

Acknowledgments

We thank the Caenorhabditis Genetics Center (funded by the NIH Office of Research Infrastructure Programs (P40 OD010440)) for providing the strains used in this study.

Funding

This work was supported by the following grants: Anusandhan National Research Foundation (ANRF) Core Research Grant (Ref. No. CRG/2023/001136) awarded by DST, India; Har-Gobind Khorana-Innovative Young Biotechnologist Fellowship (File No. HRD-17011/2/2023-HRD-DBT) and Ramalingaswami Re-entry Fellowship (Ref. No. BT/RLF/Re-entry/50/2020) awarded by the Department of Biotechnology, India; STARS grant (File No. MoE-STARS/STARS-2/2023-0116) awarded by the Ministry of Education, India; Research Grant (Ref. No. 37/1741/23/EMR-II) awarded by the Council of Scientific & Industrial Research (CSIR), India; and IISER Mohali intramural funds. P.D. was supported by a senior research fellowship from the CSIR, India.

Author Contributions

P.D. and J.S. conceived and designed the experiments. P.D. and Ravi performed the experiments. P.D. and J.S. analyzed the data and wrote the paper.

Declaration of interests

The authors declare no competing interests.

Data availability

The RNA sequencing data for N2 worms grown on the wild-type, Δ*tktA*, Δ*pdeI*, Δ*yciA*, and Δ*allD E. coli* BW25113 have been submitted to the public repository, the Sequence Read Archive, with BioProject ID PRJNA1219049. All data generated or analyzed during this study are included in the manuscript and supporting files.

References:

Ast T, Meisel JD, Patra S, Wang H, Grange RMH, Kim SH, Calvo SE, Orefice LL, Nagashima F, Ichinose F, Zapol WM, Ruvkun G, Barondeau DP, Mootha VK. 2019. Hypoxia Rescues Frataxin Loss by Restoring Iron Sulfur Cluster Biogenesis. *Cell* **177**:1507-1521.e16. doi:10.1016/j.cell.2019.03.045

Baba T, Ara T, Hasegawa M, Takai Y, Okumura Y, Baba M, Datsenko KA, Tomita M, Wanner BL, Mori H. 2006. Construction of Escherichia coli K-12 in-frame, single-gene knockout mutants: the Keio collection. *Mol Syst Biol* **2**:2006.0008. doi:10.1038/msb4100050

Bennett CF, Kaeberlein M. 2014. The mitochondrial unfolded protein response and increased longevity: Cause, consequence, or correlation? *Exp Gerontol* **0**:142–146. doi:10.1016/j.exger.2014.02.002

Bhat A, Cox RL, Hendrickson BG, Das NK, Schaller ML, Tuckowski AM, Wang E, Shah YM, Leiser SF. 2024. A diet of oxidative stress–adapted bacteria improves stress resistance and lifespan in *C. elegans* via p38-MAPK. *Sci Adv* **10**:eadk8823. doi:10.1126/sciadv.adk8823

Biagi E, Rampelli S, Turroni S, Quercia S, Candela M, Brigidi P. 2017. The gut microbiota of centenarians: Signatures of longevity in the gut microbiota profile. *Mech Ageing Dev* **165**:180–184. doi:10.1016/j.mad.2016.12.013

Blackwell TK, Steinbaugh MJ, Hourihan JM, Ewald CY, Isik M. 2015. SKN-1/Nrf, stress responses, and aging in Caenorhabditis elegans. *Free Radic Biol Med* **88**:290–301. doi:10.1016/j.freeradbiomed.2015.06.008

Brock TJ, Browse J, Watts JL. 2007. Fatty acid desaturation and the regulation of adiposity in Caenorhabditis elegans. *Genetics* **176**:865–875. doi:10.1534/genetics.107.071860

Castillo-Quan JI, Steinbaugh MJ, Fernández-Cárdenas LP, Pohl NK, Wu Z, Zhu F, Moroz N, Teixeira V, Bland MS, Lehrbach NJ, Moronetti L, Teufl M, Blackwell TK. 2023. An antisteatosis response regulated by oleic acid through lipid droplet–mediated ERAD enhancement. *Sci Adv* **9**:eadc8917. doi:10.1126/sciadv.adc8917

Chmielewski PP, Data K, Strzelec B, Farzaneh M, Anbiyaiee A, Zaheer U, Uddin S, Sheykhi-Sabzehpoush M, Mozdziak P, Zabel M, Dzięgiel P, Kempisty B. 2024. Human Aging and Age-Related Diseases: From Underlying Mechanisms to Pro-Longevity Interventions. *Aging Dis* 0. doi:10.14336/AD.2024.0280

Choi J-Y, Stukey J, Hwang S-Y, Martin CE. 1996. Regulatory Elements That Control Transcription Activation and Unsaturated Fatty Acid-mediated Repression of the *Saccharomyces cerevisiae OLE1* Gene (∗). *J Biol Chem* **271**:3581–3589. doi:10.1074/jbc.271.7.3581

Das P, Aballay A, Singh J. 2024. Calcineurin inhibition enhances Caenorhabditis elegans lifespan by defecation defects-mediated calorie restriction and nuclear hormone signaling. *eLife* **12**. doi:10.7554/eLife.89572.2

Debnath N, Kumar R, Kumar A, Mehta PK, Yadav AK. 2021. Gut-microbiota derived bioactive metabolites and their functions in host physiology. *Biotechnol Genet Eng Rev* **37**:105–153. doi:10.1080/02648725.2021.1989847

Feng M, Gao B, Garcia LR, Sun Q. 2023. Microbiota-derived metabolites in regulating the development and physiology of Caenorhabditis elegans. *Front Microbiol* **14**:1035582. doi:10.3389/fmicb.2023.1035582

Galaris D, Barbouti A, Pantopoulos K. 2019. Iron homeostasis and oxidative stress: An intimate relationship. *Biochim Biophys Acta BBA - Mol Cell Res* **1866**:118535. doi:10.1016/j.bbamcr.2019.118535

Ghosh A, Singh J. 2024. Translation initiation or elongation inhibition triggers contrasting effects on Caenorhabditis elegans survival during pathogen infection. *mBio* **15**:e02485-24. doi:10.1128/mbio.02485-24

Gokul G, Singh J. 2022. Dithiothreitol causes toxicity in *C. elegans* by modulating the methionine–homocysteine cycle. *eLife* **11**:e76021. doi:10.7554/eLife.76021

Gong J, Liu S, Wang S, Ruan H, Mou Q, Fan P, Chen T, Cai W, Lu Y, Lu Z. 2023. Identification of fecal microbiome signatures associated with familial longevity and candidate metabolites for healthy aging. *Aging Cell* **22**:e13848. doi:10.1111/acel.13848

Han B, Sivaramakrishnan P, Lin C-CJ, Neve IAA, He J, Tay LWR, Sowa JN, Sizovs A, Du G, Wang J, Herman C, Wang MC. 2017. Microbial Genetic Composition Tunes Host Longevity. *Cell* **169**:1249-1262.e13. doi:10.1016/j.cell.2017.05.036

Han H-F, Nien S-F, Jiang H-S, Wu J-C, Chiang C-Y, Li M-T, Huang L-J, Chiang S, Lin L-C, Chuang Y-T, Lin Y-H, Wang C-W, Wu Y-C. 2024. Dietary bacteria control *C. elegans* fat content through pathways converging at phosphatidylcholine. *eLife* **13**. doi:10.7554/eLife.96473.1

Han S, Schroeder EA, Silva-García CG, Hebestreit K, Mair WB, Brunet A. 2017. Mono-unsaturated fatty acids link H3K4me3 modifiers to *C. elegans* lifespan. *Nature* **544**:185–190. doi:10.1038/nature21686

Heberle H, Meirelles GV, da Silva FR, Telles GP, Minghim R. 2015. InteractiVenn: a web-based tool for the analysis of sets through Venn diagrams. *BMC Bioinformatics* **16**:169. doi:10.1186/s12859-015-0611-3

Hoeven R van der, McCallum KC, Cruz MR, Garsin DA. 2011. Ce-Duox1/BLI-3 Generated Reactive Oxygen Species Trigger Protective SKN-1 Activity via p38 MAPK Signaling during Infection in *C. elegans*. *PLOS Pathog* **7**:e1002453. doi:10.1371/journal.ppat.1002453

Hwang AB, Ryu E-A, Artan M, Chang H-W, Kabir MH, Nam H-J, Lee D, Yang J-S, Kim S, Mair WB, Lee C, Lee SS, Lee S-J. 2014. Feedback regulation via AMPK and HIF-1 mediates ROS-dependent longevity in Caenorhabditis elegans. *Proc Natl Acad Sci* **111**:E4458–E4467. doi:10.1073/pnas.1411199111

Inoue H, Hisamoto N, An JH, Oliveira RP, Nishida E, Blackwell TK, Matsumoto K. 2005. The *C. elegans* p38 MAPK pathway regulates nuclear localization of the transcription factor SKN-1 in oxidative stress response. *Genes Dev* **19**:2278–2283. doi:10.1101/gad.1324805

Jenkins NL, James SA, Salim A, Sumardy F, Speed TP, Conrad M, Richardson DR, Bush AI, McColl G. 2020. Changes in ferrous iron and glutathione promote ferroptosis and frailty in aging Caenorhabditis elegans. *eLife* **9**:e56580. doi:10.7554/eLife.56580

Kennedy BK, Berger SL, Brunet A, Campisi J, Cuervo AM, Epel ES, Franceschi C, Lithgow GJ, Morimoto RI, Pessin JE, Rando TA, Richardson A, Schadt EE, Wyss-Coray T, Sierra F. 2014. Geroscience: linking aging to chronic disease. *Cell* **159**:709–713. doi:10.1016/j.cell.2014.10.039

Kenyon CJ. 2010. The genetics of ageing. *Nature* **464**:504–512. doi:10.1038/nature08980

Khanna A, Kumar J, Vargas MA, Barrett L, Katewa S, Li P, McCloskey T, Sharma A, Naudé N, Nelson C, Brem R, Killilea DW, Mooney SD, Gill M, Kapahi P. 2016. A genome-wide screen of bacterial mutants that enhance dauer formation in *C. elegans*. *Sci Rep* **6**:38764. doi:10.1038/srep38764

Kim J, Jo Y, Cho D, Ryu D. 2022. L-threonine promotes healthspan by expediting ferritin-dependent ferroptosis inhibition in *C. elegans*. *Nat Commun* **13**:6554. doi:10.1038/s41467-022-34265-x

Lee S-J, Hwang AB, Kenyon C. 2010. Inhibition of Respiration Extends *C. elegans* Life Span via Reactive Oxygen Species that Increase HIF-1 Activity. *Curr Biol* **20**:2131–2136. doi:10.1016/j.cub.2010.10.057

Li Z, Zhang Z, Ren Y, Wang Y, Fang J, Yue H, Ma S, Guan F. 2021. Aging and age-related diseases: from mechanisms to therapeutic strategies. *Biogerontology* **22**:165–187. doi:10.1007/s10522-021-09910-5

Lin X-X, Sen I, Janssens GE, Zhou X, Fonslow BR, Edgar D, Stroustrup N, Swoboda P, Yates JR, Ruvkun G, Riedel CG. 2018. DAF-16/FOXO and HLH-30/TFEB function as combinatorial transcription factors to promote stress resistance and longevity. *Nat Commun* **9**:4400. doi:10.1038/s41467-018-06624-0

López-Otín C, Blasco MA, Partridge L, Serrano M, Kroemer G. 2013. The Hallmarks of Aging. *Cell* **153**:1194–1217. doi:10.1016/j.cell.2013.05.039

Mack HID, Heimbucher T, Murphy CT. 2018. The nematode *Caenorhabditis elegans* as a model for aging research. *Drug Discov Today Dis Models*, Models for Aging Research **27**:3–13. doi:10.1016/j.ddmod.2018.11.001

MacNeil LT, Watson E, Arda HE, Zhu LJ, Walhout AJM. 2013. Diet-Induced Developmental Acceleration Independent of TOR and Insulin in *C. elegans*. *Cell* **153**:240–252. doi:10.1016/j.cell.2013.02.049

Masoro EJ. 2005. Overview of caloric restriction and ageing. *Mech Ageing Dev*, Dietary restriction, longevity and ageing - the current state of our knowledge and ignorance **126**:913–922. doi:10.1016/j.mad.2005.03.012

Melber A, Haynes CM. 2018. UPRmt regulation and output: a stress response mediated by mitochondrial-nuclear communication. *Cell Res* **28**:281–295. doi:10.1038/cr.2018.16

Molinero N, Antón-Fernández A, Hernández F, Ávila J, Bartolomé B, Moreno-Arribas MV. 2023. Gut Microbiota, an Additional Hallmark of Human Aging and Neurodegeneration. *Neuroscience* **518**:141–161. doi:10.1016/j.neuroscience.2023.02.014

Naim N, Amrit FRG, Ratnappan R, DelBuono N, Loose JA, Ghazi A. 2021. Cell nonautonomous roles of NHR-49 in promoting longevity and innate immunity. *Aging Cell* **20**:e13413. doi:10.1111/acel.13413

Nargund AM, Pellegrino MW, Fiorese CJ, Baker BM, Haynes CM. 2012. Mitochondrial Import Efficiency of ATFS-1 Regulates Mitochondrial UPR Activation. *Science* **337**:587–590. doi:10.1126/science.1223560

Ntambi JM, Miyazaki M. 2003. Recent insights into stearoyl-CoA desaturase-1. *Curr Opin Lipidol* **14**:255.

Paek J, Lo JY, Narasimhan SD, Nguyen TN, Glover-Cutter K, Robida-Stubbs S, Suzuki T, Yamamoto M, Blackwell TK, Curran SP. 2012. Mitochondrial SKN-1/Nrf Mediates a Conserved Starvation Response. *Cell Metab* **16**:526–537. doi:10.1016/j.cmet.2012.09.007

Ragonnaud E, Biragyn A. 2021. Gut microbiota as the key controllers of “healthy” aging of elderly people. *Immun Ageing* **18**:2. doi:10.1186/s12979-020-00213-w

Rao R, Aballay A, Singh J. 2024. Inhibition of the UFD-1-NPL-4 complex triggers an inflammation-like response in Caenorhabditis elegans. *eLife* **13**. doi:10.7554/eLife.94310.1

Ratnappan R, Amrit FRG, Chen S-W, Gill H, Holden K, Ward J, Yamamoto KR, Olsen CP, Ghazi A. 2014. Germline Signals Deploy NHR-49 to Modulate Fatty-Acid β-Oxidation and Desaturation in Somatic Tissues of *C. elegans*. *PLOS Genet* **10**:e1004829. doi:10.1371/journal.pgen.1004829

Ravi, Kumar A, Bhattacharyya S, Singh J. 2023. Thiol reductive stress activates the hypoxia response pathway. *EMBO J* **42**:e114093. doi:10.15252/embj.2023114093

Ravi, Singh J. 2025. Redox imbalance and hypoxia-inducible factors: a multifaceted crosstalk. *FEBS J*. doi:10.1111/febs.70013

Reis RJS, Xu L, Lee H, Chae M, Thaden JJ, Bharill P, Tazearslan C, Siegel E, Alla R, Zimniak P, Ayyadevara S. 2011. Modulation of lipid biosynthesis contributes to stress resistance and longevity of *C. elegans* mutants. *Aging* **3**:125–147. doi:10.18632/aging.100275

Rooks MG, Garrett WS. 2016. Gut microbiota, metabolites and host immunity. *Nat Rev Immunol* **16**:341–352. doi:10.1038/nri.2016.42

Schaar CE, Dues DJ, Spielbauer KK, Machiela E, Cooper JF, Senchuk M, Hekimi S, Raamsdonk JMV. 2015. Mitochondrial and Cytoplasmic ROS Have Opposing Effects on Lifespan. *PLOS Genet* **11**:e1004972. doi:10.1371/journal.pgen.1004972

Schiavi A, Maglioni S, Palikaras K, Shaik A, Strappazzon F, Brinkmann V, Torgovnick A, Castelein N, De Henau S, Braeckman BP, Cecconi F, Tavernarakis N, Ventura N. 2015. Iron-Starvation-Induced Mitophagy Mediates Lifespan Extension upon Mitochondrial Stress in *C. elegans*. *Curr Biol* **25**:1810–1822. doi:10.1016/j.cub.2015.05.059

Schiavi A, Salveridou E, Brinkmann V, Shaik A, Menzel R, Kalyanasundaram S, Nygård S, Nilsen H, Ventura N. 2023. Mitochondria hormesis delays aging and associated diseases in Caenorhabditis elegans impacting on key ferroptosis players. *iScience* **26**. doi:10.1016/j.isci.2023.106448

Schiavi A, Torgovnick A, Kell A, Megalou E, Castelein N, Guccini I, Marzocchella L, Gelino S, Hansen M, Malisan F, Condò I, Bei R, Rea SL, Braeckman BP, Tavernarakis N, Testi R, Ventura N. 2013. Autophagy induction extends lifespan and reduces lipid content in response to frataxin silencing in *C. elegans*. *Exp Gerontol* **48**:191–201. doi:10.1016/j.exger.2012.12.002

Schroeder EA, Brunet A. 2015. Lipid Profiles and Signals for Long Life. *Trends Endocrinol Metab TEM* **26**:589–592. doi:10.1016/j.tem.2015.08.007

Schulz TJ, Zarse K, Voigt A, Urban N, Birringer M, Ristow M. 2007. Glucose Restriction Extends *Caenorhabditis elegans* Life Span by Inducing Mitochondrial Respiration and Increasing Oxidative Stress. *Cell Metab* **6**:280–293. doi:10.1016/j.cmet.2007.08.011

Selman C. 2014. Dietary restriction and the pursuit of effective mimetics. *Proc Nutr Soc* **73**:260–270. doi:10.1017/S0029665113003832

Sheng Y, Yang G, Casey K, Curry S, Oliver M, Han SM, Leeuwenburgh C, Xiao R. 2021. A novel role of the mitochondrial iron-sulfur cluster assembly protein ISCU-1/ISCU in longevity and stress response. *GeroScience* **43**:691–707. doi:10.1007/s11357-021-00327-z

Shi P, Xu S, Yang Z, Wang L, Wu Y, Li Y, Zhu Z. 2024. Harnessing gut microbiota for longevity: Insights into mechanisms and genetic manipulation. *iMetaOmics* **1**:e36. doi:10.1002/imo2.36

Shin M-G, Lee J-W, Han J-S, Lee B, Jeong J-H, Park S-H, Kim J-H, Jang S, Park M, Kim S-Y, Kim S, Yang YR, Kim J-Y, Hoe K-L, Park C, Lee K-P, Kwon K-S, Kwon E-S. 2020. Bacteria-derived metabolite, methylglyoxal, modulates the longevity of *C. elegans* through TORC2/SGK-1/DAF-16 signaling. *Proc Natl Acad Sci* **117**:17142–17150. doi:10.1073/pnas.1915719117

Shpilka T, Haynes CM. 2018. The mitochondrial UPR: mechanisms, physiological functions and implications in ageing. *Nat Rev Mol Cell Biol* **19**:109–120. doi:10.1038/nrm.2017.110

Smith P, Willemsen D, Popkes M, Metge F, Gandiwa E, Reichard M, Valenzano DR. 2017. Regulation of life span by the gut microbiota in the short-lived African turquoise killifish. *eLife* **6**:e27014. doi:10.7554/eLife.27014

Speakman JR, Mitchell SE. 2011. Caloric restriction. *Mol Aspects Med*, Caloric Restriction **32**:159–221. doi:10.1016/j.mam.2011.07.001

Turner CD, Ramos CM, Curran SP. 2024. Disrupting the SKN-1 homeostat: mechanistic insights and phenotypic outcomes. *Front Aging* **5**. doi:10.3389/fragi.2024.1369740

Venkatesh SR, Siddiqui R, Sandhu A, Ramani M, Houston IR, Watts JL, Singh V. 2023. Homeostatic control of stearoyl desaturase expression via patched-like receptor PTR-23 ensures the survival of *C. elegans* during heat stress. *PLOS Genet* **19**:e1011067. doi:10.1371/journal.pgen.1011067

Virk B, Jia J, Maynard CA, Raimundo A, Lefebvre J, Richards SA, Chetina N, Liang Y, Helliwell N, Cipinska M, Weinkove D. 2016. Folate Acts in *E. coli* to Accelerate *C. elegans* Aging

Independently of Bacterial Biosynthesis. *Cell Rep* **14**:1611–1620. doi:10.1016/j.celrep.2016.01.051

Walker AK, See R, Batchelder C, Kophengnavong T, Gronniger JT, Shi Y, Blackwell TK. 2000. A Conserved Transcription Motif Suggesting Functional Parallels between Caenorhabditis elegans SKN-1 and Cap'n'Collar-related Basic Leucine Zipper Proteins *. *J Biol Chem* **275**:22166–22171. doi:10.1074/jbc.M001746200

Wang H, Chen W, Lei L, Zhang W, Liu Z, Wang Y, Xu B. 2024. Queen bee gut microbiota extends honeybee lifespan by inhibiting insulin signaling. *Appl Environ Microbiol* **90**:e01799-23. doi:10.1128/aem.01799-23

Wang J, Pantopoulos K. 2011. Regulation of cellular iron metabolism. *Biochem J* **434**:365–381. doi:10.1042/BJ20101825

Watts JL, Browse J. 2002. Genetic dissection of polyunsaturated fatty acid synthesis in Caenorhabditis elegans. *Proc Natl Acad Sci* **99**:5854–5859. doi:10.1073/pnas.092064799

Wei Y, Kenyon C. 2016. Roles for ROS and hydrogen sulfide in the longevity response to germline loss in Caenorhabditis elegans. *Proc Natl Acad Sci* **113**:E2832–E2841. doi:10.1073/pnas.1524727113

Xin N, Durieux J, Yang C, Wolff S, Kim H-E, Dillin A. 2022. The UPRmt preserves mitochondrial import to extend lifespan. *J Cell Biol* **221**:e202201071. doi:10.1083/jcb.202201071

Yang W, Hekimi S. 2010. A Mitochondrial Superoxide Signal Triggers Increased Longevity in Caenorhabditis elegans. *PLOS Biol* **8**:e1000556. doi:10.1371/journal.pbio.1000556

Yoneda T, Benedetti C, Urano F, Clark SG, Harding HP, Ron D. 2004. Compartment-specific perturbation of protein handling activates genes encoding mitochondrial chaperones. *J Cell Sci* **117**:4055–4066. doi:10.1242/jcs.01275

Zhang J, Holdorf AD, Walhout AJM. 2017. *C. elegans* and its bacterial diet as a model for systems-level understanding of host-microbiota interactions. *Curr Opin Biotechnol* **46**:74–80. doi:10.1016/j.copbio.2017.01.008

Zhang J, Li X, Olmedo M, Holdorf AD, Shang Y, Artal-Sanz M, Yilmaz LS, Walhout AJM. 2019. A Delicate Balance between Bacterial Iron and Reactive Oxygen Species Supports Optimal *C. elegans* Development. *Cell Host Microbe* **26**:400-411.e3. doi:10.1016/j.chom.2019.07.010

Figures

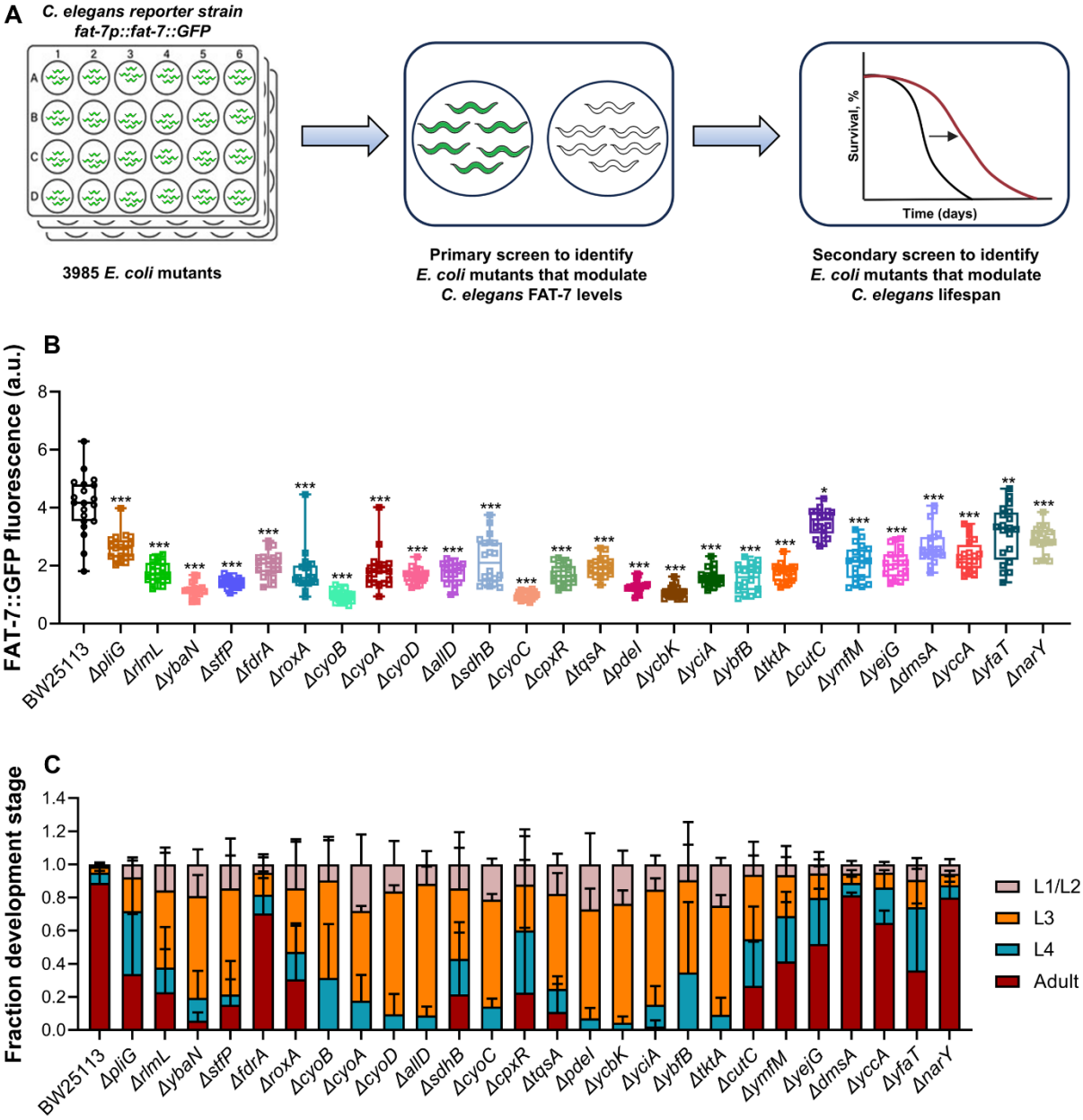

Figure 1. Genome-wide bacterial screen identifies *E. coli* mutants that modulate *C. elegans* FAT-7 levels

(A) Schematic representation of the genome-wide primary bacterial screen used to identify *E. coli* mutants that modulate *C. elegans* FAT-7 levels, followed by a secondary screen to assess their impact on lifespan.

(B) Quantification of GFP levels of *fat-7p::fat-7::GFP* worms grown on *E. coli* BW25113 and mutant diets. ***$p < 0.001$, **$p < 0.01$, and *$p < 0.05$ via the *t*-test ($n = 20$ worms each).

(C) Quantification of different developmental stages of N2 worms grown on *E. coli* BW25113 and mutant diets at 20°C, 60 hours after transferring synchronized L1 larvae ($n = 3$ biological replicates; animals per condition per replicate >45).

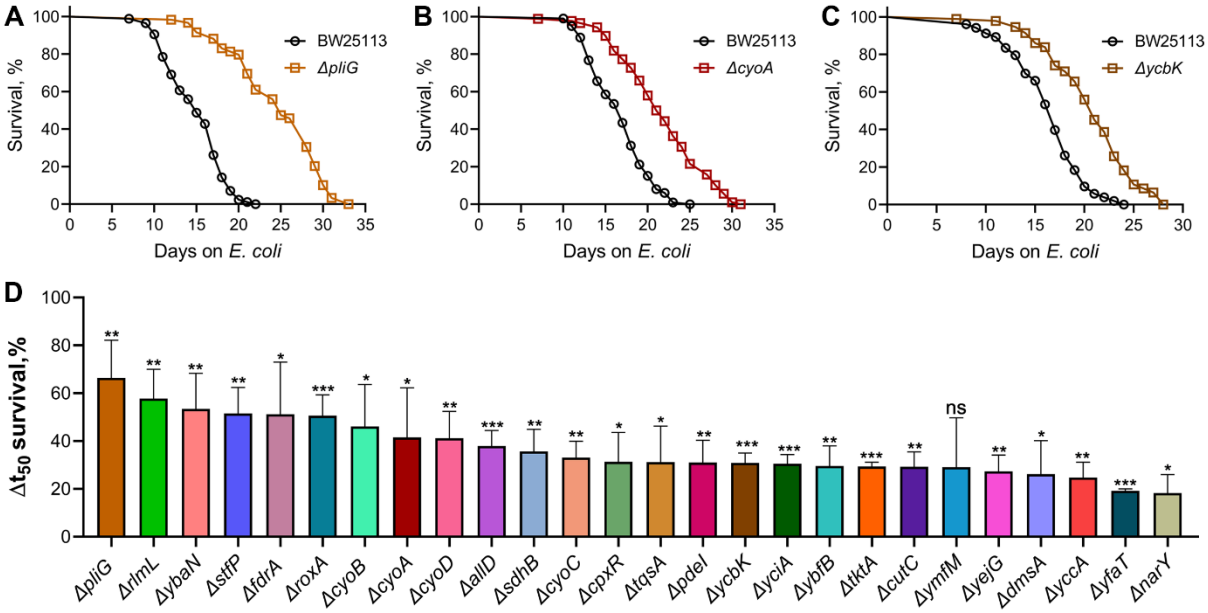

Figure 2. *E. coli* mutants that decrease FAT-7 levels extend *C. elegans* lifespan

(A)-(C) Representative survival curves of N2 worms fed on *E. coli* mutants *ΔpliG* (A), *ΔcyoA* (B), and *ΔycbK* (C), along with the BW25113 controls. $p < 0.001$ for all the plots (n = 3 biological replicates; animals per condition per replicate > 58).

(D) The percent change in mean survival of N2 worms fed on *E. coli* mutant diets relative to the BW25113 control. ***$p < 0.001$, **$p < 0.01$, and *$p < 0.05$ via the *t*-test. ns, nonsignificant. Data represent the mean and standard deviation from three independent experiments.

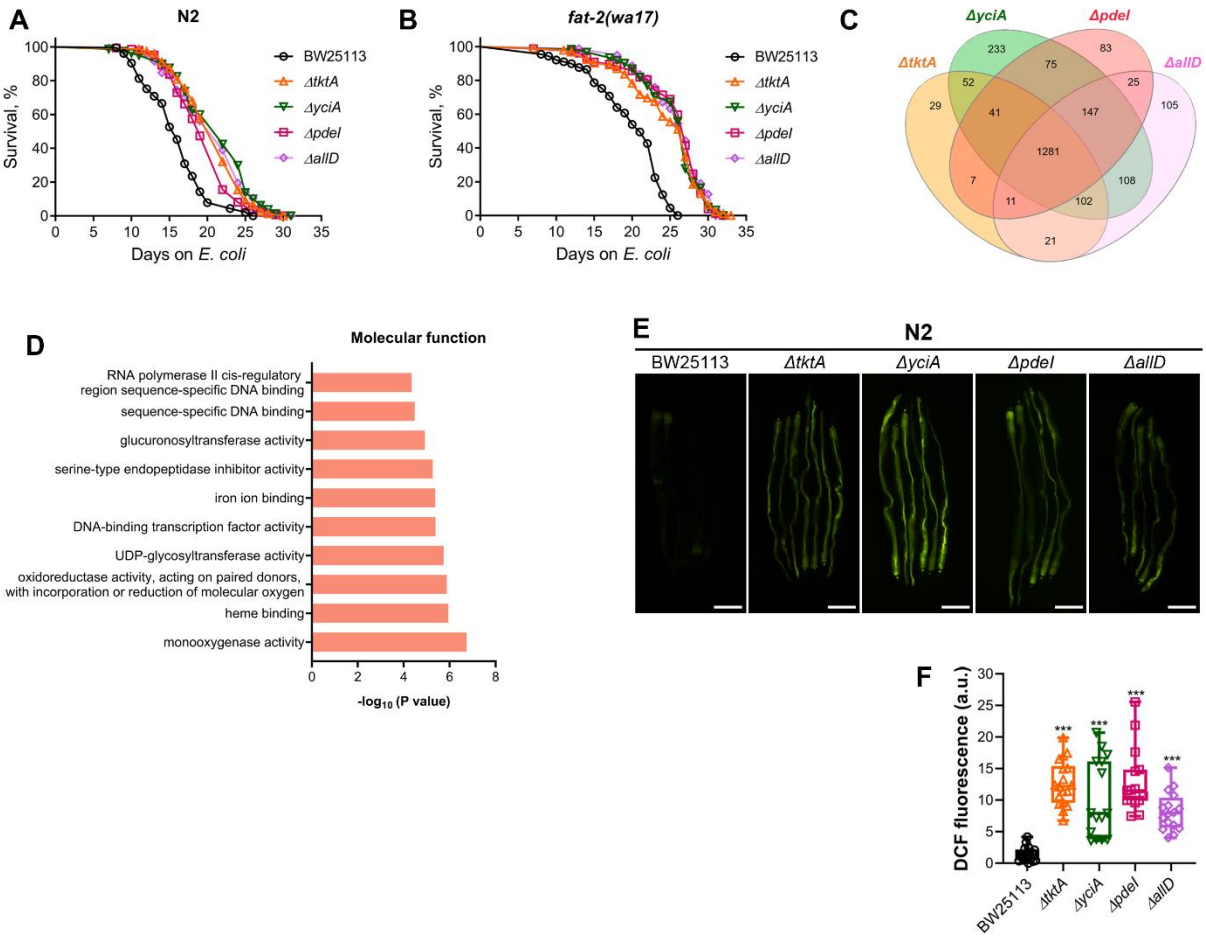

Figure 3. Mutant *E. coli* diets induce oxidative stress in *C. elegans*

(A) Representative survival curves of N2 worms fed on *ΔtktA*, *ΔyciA*, *ΔpdeI*, and *ΔallD E. coli* mutants along with the BW25113 control. $p < 0.001$ for all the mutant diets compared to the BW25113 control (n = 3 biological replicates; animals per condition per replicate > 75).

(B) Representative survival curves of *fat-2(wa17)* worms fed on *ΔtktA*, *ΔyciA*, *ΔpdeI*, and *ΔallD E. coli* mutants along with the BW25113 control. $p < 0.001$ for all the mutant diets compared to the BW25113 control (n = 3 biological replicates; animals per condition per replicate > 60).

(C) Venn diagram showing the overlap of upregulated genes in N2 worms fed on Δ*tktA*, Δ*yciA*, Δ*pdeI*, and Δ*allD E. coli* mutants compared to the BW25113 control.

(D) Gene ontology enrichment analysis of molecular function for the common 1,281 genes upregulated in N2 worms grown on *E. coli* mutants *ΔtktA*, *ΔyciA*, *ΔpdeI*, and *ΔallD*.

(E) Representative fluorescence images of N2 worms grown on *ΔtktA*, *ΔyciA*, *ΔpdeI*, and *ΔallD E. coli* mutants along with the BW25113 control and exposed to 2′,7′-dichlorofluorescein diacetate for 5 hours before imaging. Scale bar = 200 µm.

(F) Quantification of fluorescence levels of 2′,7′-dichlorofluorescein (DCF) in N2 worms grown on *ΔtktA*, *ΔyciA*, *ΔpdeI*, and *ΔallD E. coli* mutants along with the BW25113 control and exposed to 2′, 7′-dichlorodihydrofluoroscein diacetate for 5 hours before imaging. ***$p < 0.001$ via the *t*-test (n = 15-18 worms each).

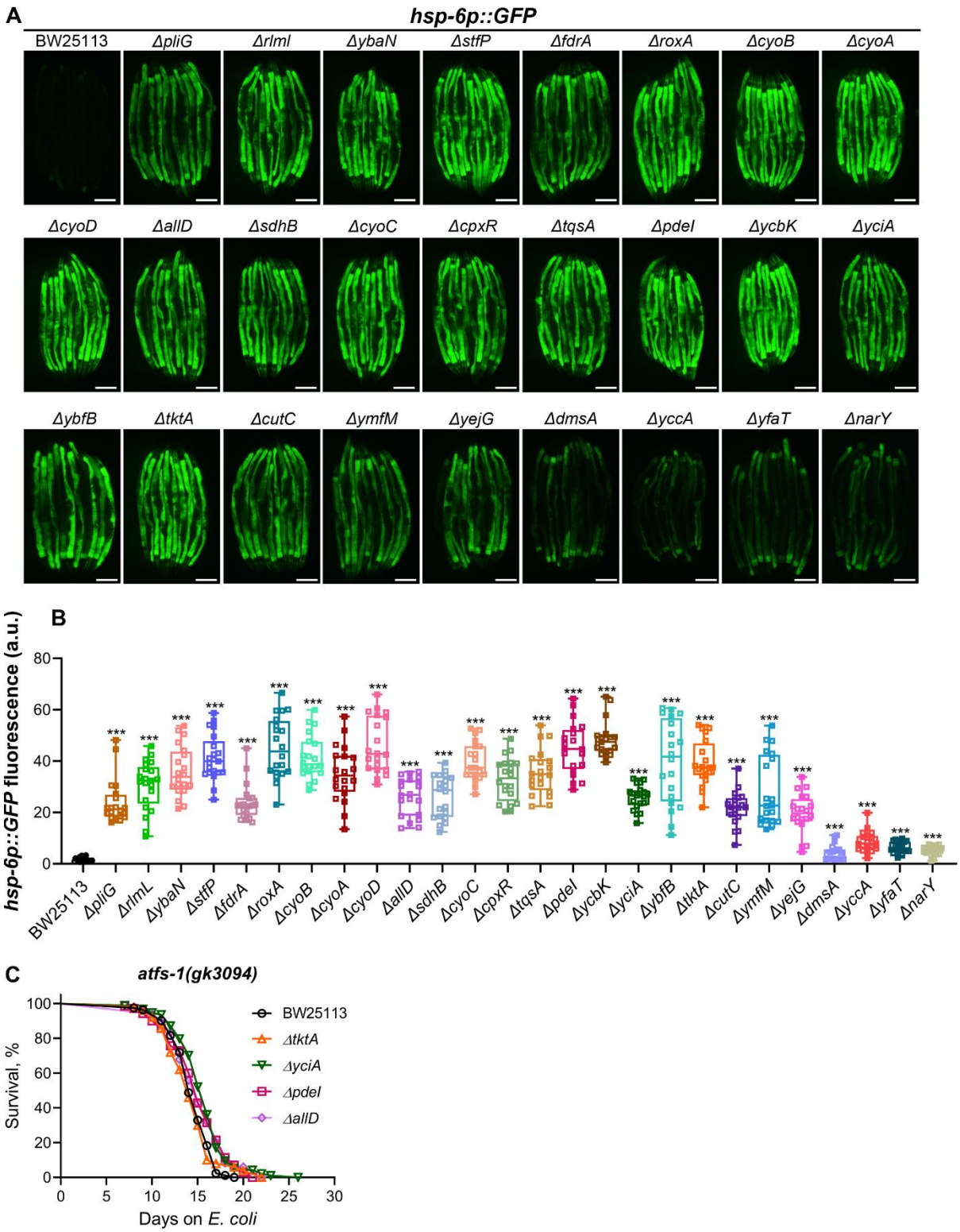

Figure 4. Mutant *E. coli* diets that suppress *C. elegans* FAT-7 activate host mitochondrial UPR

(A) Representative fluorescence images of *hsp-6p::GFP* worms grown on BW25113 and mutant *E. coli* diets. Scale bar = 200 µm.

(B) Quantification of GFP levels of *hsp-6p::GFP* worms grown on BW25113 and mutant *E. coli* diets. ***$p < 0.001$ via the *t*-test (n = 19-21 worms each).

(C) Representative survival curves of *atfs-1(gk3094)* worms fed on *ΔtktA*, *ΔyciA*, *ΔpdeI*, and *ΔallD E. coli* mutants along with the BW25113 control. $p < 0.001$ for *ΔyciA*, $p < 0.05$ for *ΔpdeI* and *ΔallD*, and nonsignificant for *ΔtktA* compared to the BW25113 control (n = 3 biological replicates; animals per condition per replicate > 54).

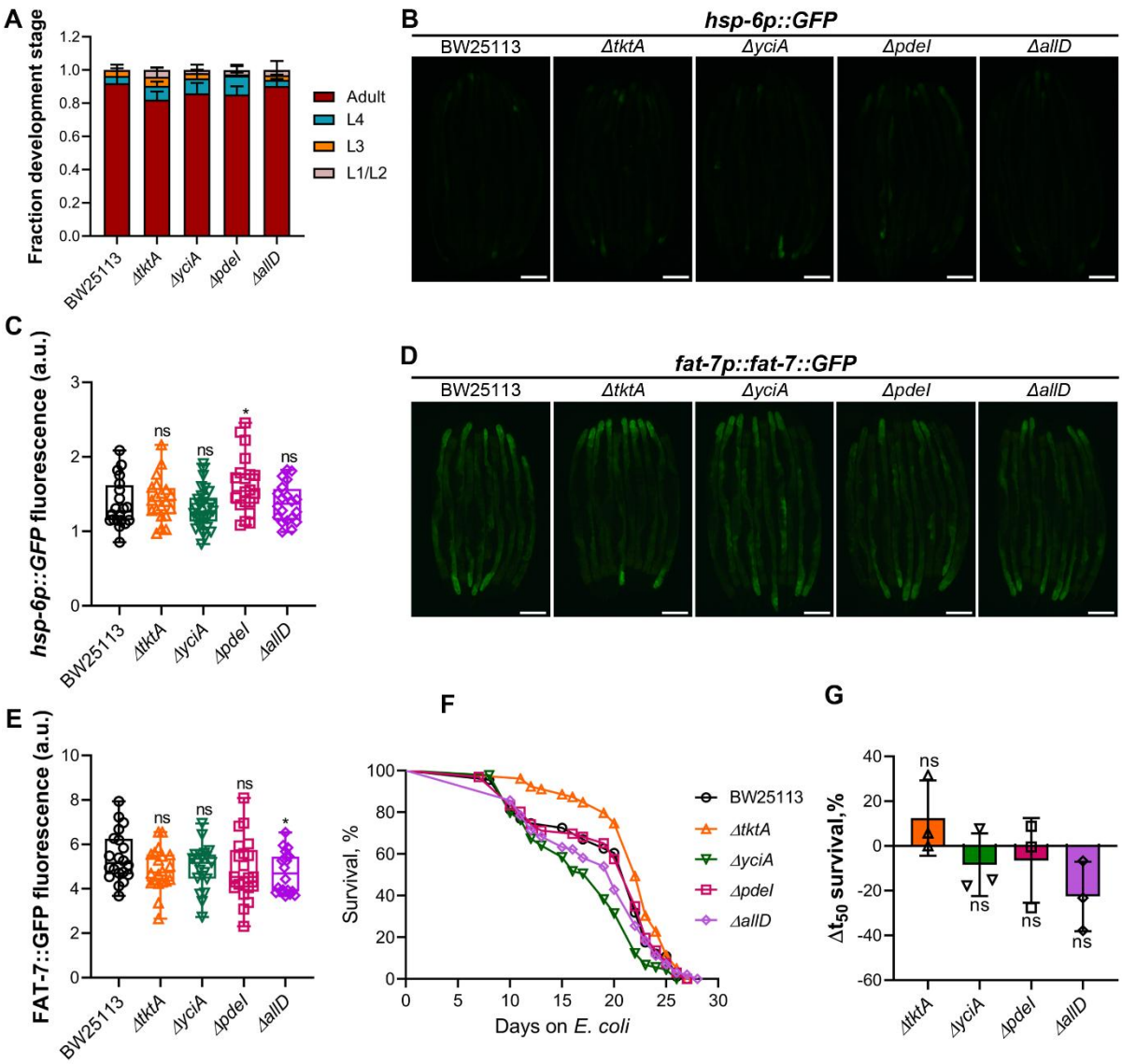

Figure 5. Iron supplementation rescues mutant diet-induced phenotypes

(A) Quantification of different developmental stages of N2 worms grown at 20°C for 60 hours after transferring synchronized L1 larvae onto *E. coli* BW25113 and mutant diets supplemented with 4 mM ferric chloride (n = 3 biological replicates; animals per condition per replicate >50).

(B) Representative fluorescence images of *hsp-6p::GFP* worms grown on BW25113 and mutant *E. coli* diets supplemented with 4 mM ferric chloride. Scale bar = 200 µm.

(C) Quantification of GFP levels of *hsp-6p::GFP* worms grown on BW25113 and mutant *E. coli* diets supplemented with 4 mM ferric chloride. *$p < 0.05$ via the t-test. ns, nonsignificant (n = 20-20 worms each).

(D) Representative fluorescence images of *fat-7p::fat-7::GFP* worms grown on BW25113 and mutant *E. coli* diets supplemented with 4 mM ferric chloride. Scale bar = 200 µm.

(E) Quantification of GFP levels of *fat-7p::fat-7::GFP* worms grown on BW25113 and mutant *E. coli* diets supplemented with 4 mM ferric chloride. *$p < 0.05$ via the t-test. ns, nonsignificant (n = 20-21 worms each).

(F) Representative survival curves of N2 worms fed on *ΔtktA*, *ΔyciA*, *ΔpdeI*, and *ΔallD E. coli* mutants along with the BW25113 control supplemented with 4 mM ferric chloride. $p < 0.05$ for *ΔtktA*, $p < 0.001$ for *ΔyciA*, and nonsignificant for *ΔpdeI* and *ΔallD* compared to the BW25113 control (n = 3 biological replicates; animals per condition per replicate > 60).

(G) The percent change in mean survival of N2 worms fed on *ΔtktA*, *ΔyciA*, *ΔpdeI*, and *ΔallD E. coli* mutants supplemented with 4 mM ferric chloride compared to the BW25113 control. ns, nonsignificant via the *t*-test. Data represent the mean and standard deviation from three independent experiments.

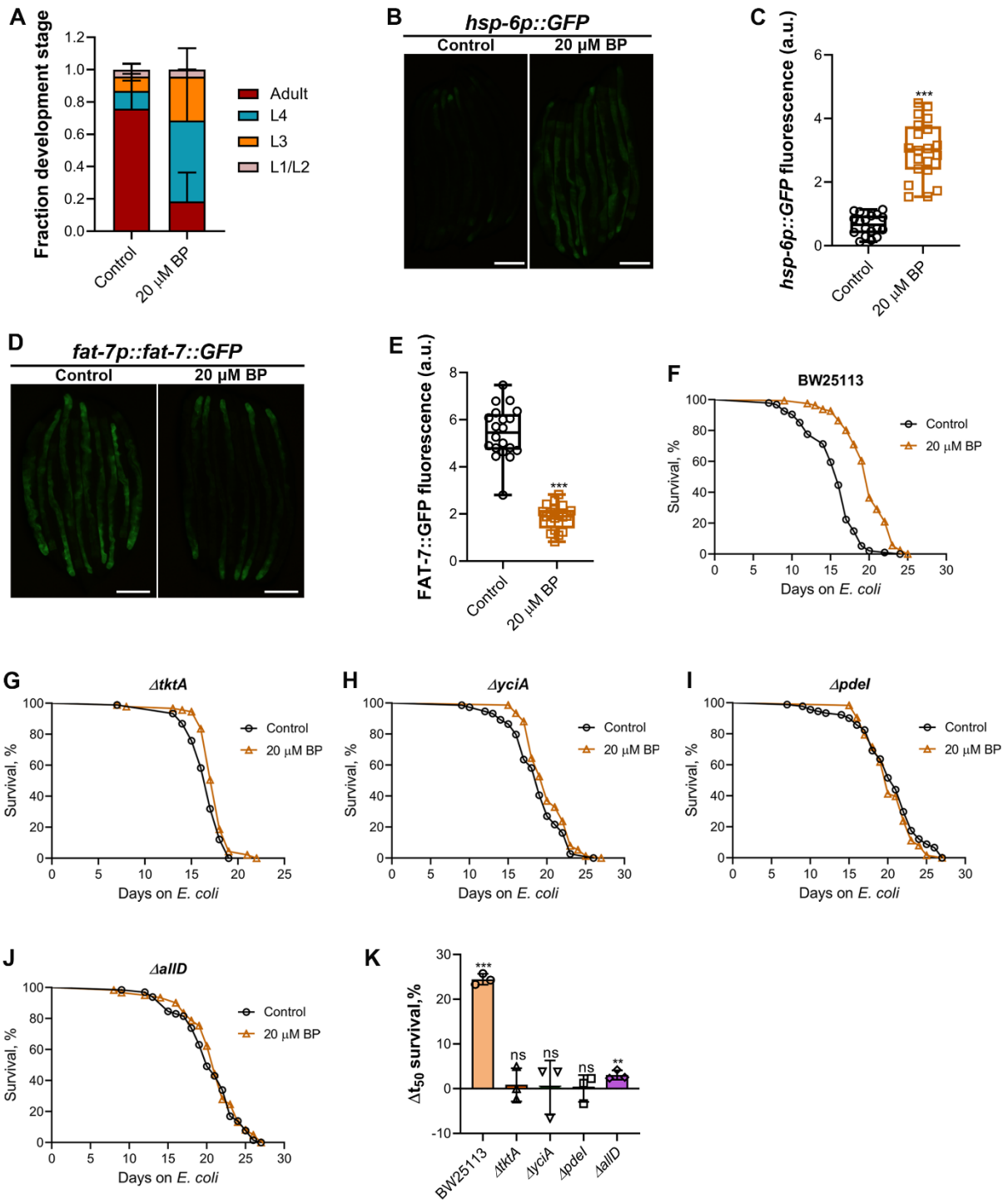

Figure 6. Low dietary iron mimics mutant diet-induced phenotypes

(A) Quantification of different developmental stages of N2 worms grown at 20°C for 60 hours after transferring synchronized L1 larvae onto *E. coli* BW25113 and mutant diets supplemented with DMSO control and 20 µM 2,2'-bipyridyl (BP) (n = 3 biological replicates; animals per condition per replicate >60).

(B) Representative fluorescence images of *hsp-6p::GFP* worms grown on *E. coli* BW25113 supplemented with DMSO control and 20 µM BP. Scale bar = 200 µm.

(C) Quantification of GFP levels of *hsp-6p::GFP* worms grown on *E. coli* BW25113 supplemented with DMSO control and 20 µM BP. ***$p < 0.001$ via the *t*-test (n = 18-20 worms each).

(D) Representative fluorescence images of *fat-7p::fat-7::GFP* worms grown on *E. coli* BW25113 supplemented with DMSO control and 20 µM BP. Scale bar = 200 µm.

(E) Quantification of GFP levels of *fat-7p::fat-7::GFP* worms grown on *E. coli* BW25113 supplemented with DMSO control and 20 µM BP. ***$p < 0.001$ via the *t*-test (n = 20 worms each).

(F)-(J) Representative survival curves of N2 worms grown on BW25113 (F), *ΔtktA* (G), *ΔyciA* (H), *ΔpdeI* (I), and *ΔallD* (J) mutant *E. coli* diets supplemented with DMSO control and 20 µM BP. $P < 0.001$ for BW25113, $p < 0.001$ for *ΔtktA* and nonsignificant for *ΔyciA*, *ΔpdeI*, and *ΔallD* (n = 3 biological replicates; animals per condition per replicate > 50).

(K) The percent change in mean survival of N2 worms grown on BW25113, *ΔtktA*, *ΔyciA*, *ΔpdeI*, and *ΔallD* mutant *E. coli* diets supplemented with 20 µM BP compared to their respective DMSO controls. ***$p < 0.001$ and **$p < 0.01$ via the *t*-test. ns, nonsignificant. Data represent the mean and standard deviation from three independent experiments.

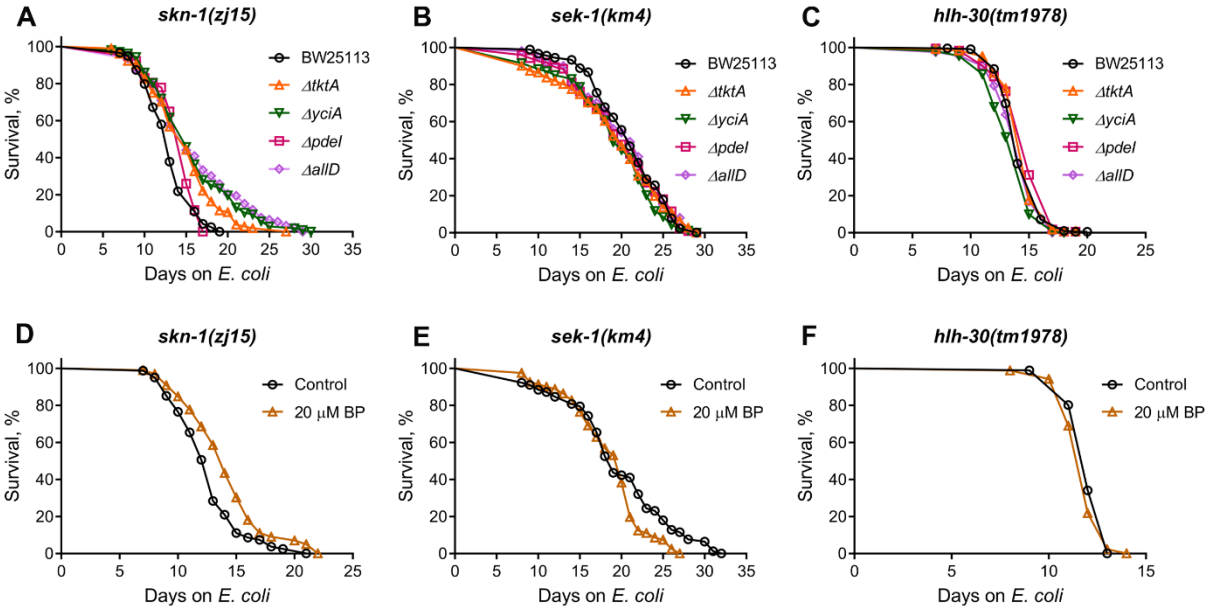

Figure 7. Lifespan extension under low dietary iron depends on oxidative stress response pathways

(A) Representative survival curves of *skn-1(zj15)* worms fed on *ΔtktA*, *ΔyciA*, *ΔpdeI*, and *ΔallD E. coli* mutants along with the BW25113 control. $p < 0.001$ for *ΔtktA*, *ΔyciA*, and *ΔallD* and $p < 0.05$ for *ΔpdeI* compared to the BW25113 control (n = 3 biological replicates; animals per condition per replicate > 70).

(B) Representative survival curves of *sek-1(km4)* worms fed on *ΔtktA*, *ΔyciA*, *ΔpdeI*, and *ΔallD E. coli* mutants along with the BW25113 control. $p < 0.05$ for *ΔyciA* and nonsignificant for *ΔtktA*, *ΔpdeI*, and *ΔallD* compared to the BW25113 control (n = 3 biological replicates; animals per condition per replicate > 60).

(C) Representative survival curves of *hlh-30(tm1978)* worms fed on *ΔtktA*, *ΔyciA*, *ΔpdeI*, and *ΔallD E. coli* mutants along with the BW25113 control. $p < 0.001$ for *ΔyciA*, $p < 0.05$ for *ΔtktA* and *ΔpdeI*, and nonsignificant for *ΔallD* compared to the BW25113 control (n = 3 biological replicates; animals per condition per replicate > 80).

(D) Representative survival curves of *skn-1(zj15)* worms grown on *E. coli* BW25113 supplemented with DMSO control and 20 µM 2,2'-bipyridyl (BP). $p < 0.001$ for BP compared to the control (n = 3 biological replicates; animals per condition per replicate > 60).

(E) Representative survival curves of *sek-1(km4)* worms grown on *E. coli* BW25113 supplemented with DMSO control and 20 µM BP. nonsignificant for BP compared to the control (n = 3 biological replicates; animals per condition per replicate > 70).

(F) Representative survival curves of *hlh-30(tm1978)* worms grown on *E. coli* BW25113 supplemented with DMSO control and 20 µM BP. nonsignificant for BP compared to the control (n = 3 biological replicates; animals per condition per replicate > 80).

Supplementary Figures

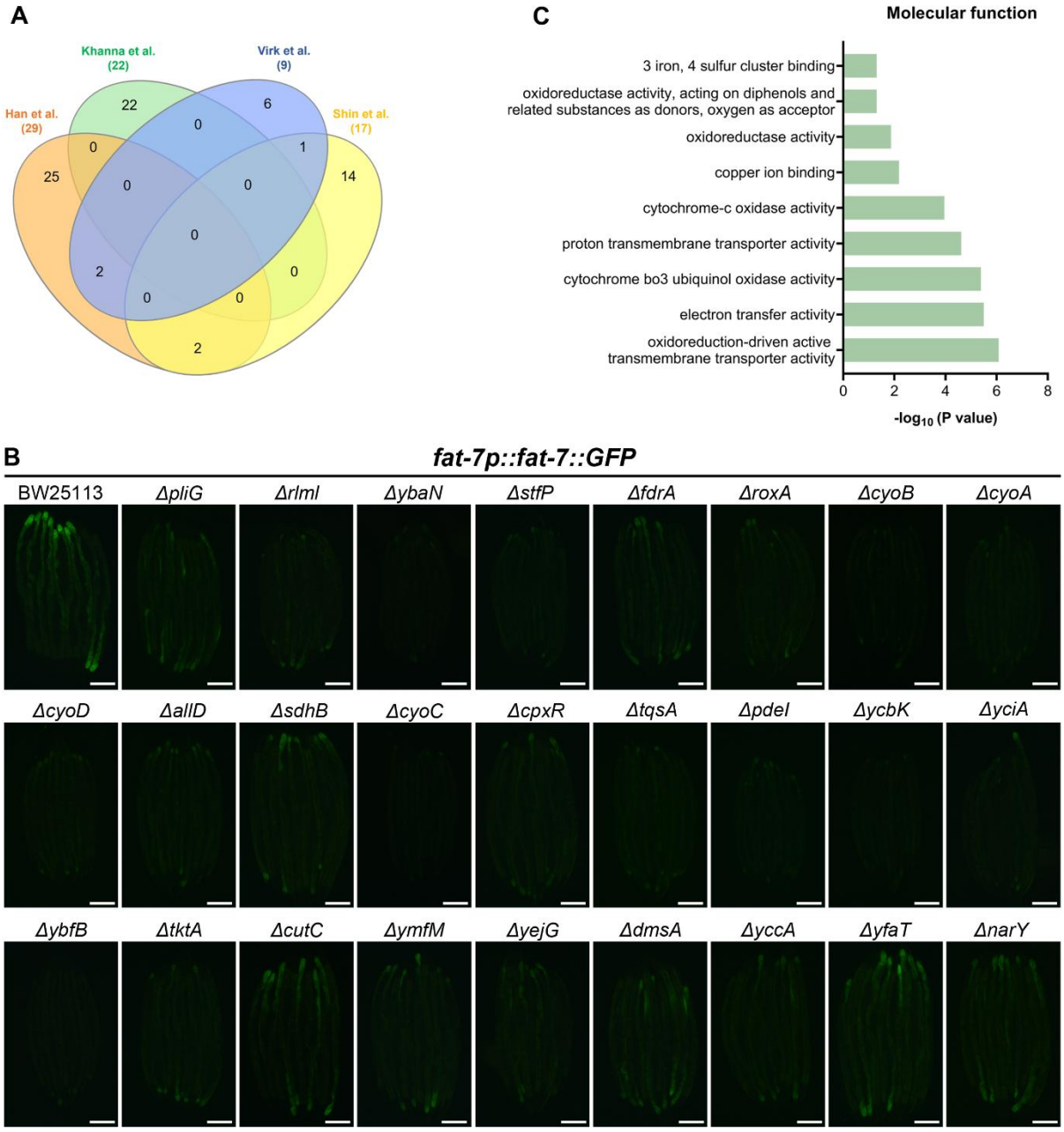

Figure S1. Genome-wide bacterial screen identifies *E. coli* mutants that modulate *C. elegans* FAT-7 levels

(A) Venn diagram showing the overlap among *E. coli* mutants identified in genome-wide bacterial screens for mutants that extend *C. elegans* lifespan (B. Han et al., 2017; Khanna et al., 2016; Shin et al., 2020; Virk et al., 2016).

(B) Representative fluorescence images of *fat-7p::fat-7::GFP* worms grown on *E. coli* BW25113 and mutant diets. Scale bar = 200 µm.

(C) Gene ontology enrichment analysis for molecular functions associated with the 26 *E. coli* mutants that downregulate *C. elegans* FAT-7 levels.

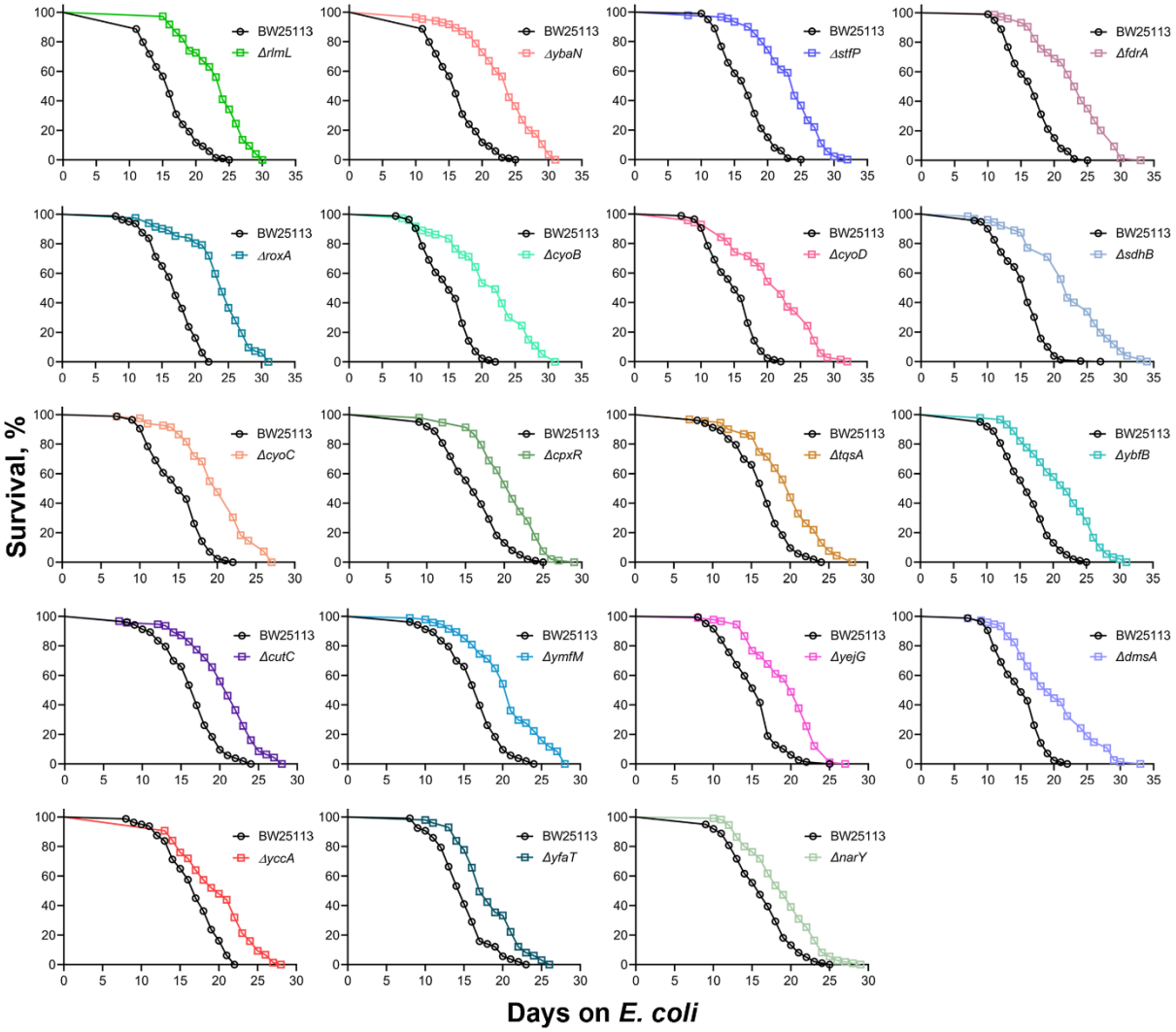

Figure S2. *E. coli* mutants that decrease FAT-7 levels extend *C. elegans* lifespan

Representative survival curves of N2 worms fed on *E. coli* BW25113 and mutants that decrease FAT-7 levels. The BW25113 control is common for different cohorts of the survival curves. The survival plot for the remaining mutants is shown in Figures 2A-C and 3A.

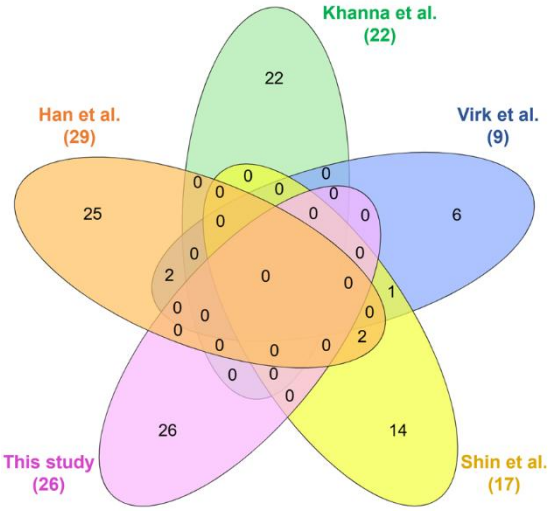

Figure S3. The pro-longevity *E. coli* mutants identified in this study differ from previously identified mutants

Venn diagram showing the overlap among *E. coli* mutants identified in previous genome-wide bacterial screens for mutants that extend *C. elegans* lifespan (B. Han et al., 2017; Khanna et al., 2016; Shin et al., 2020; Virk et al., 2016) and the mutants identified in this study.

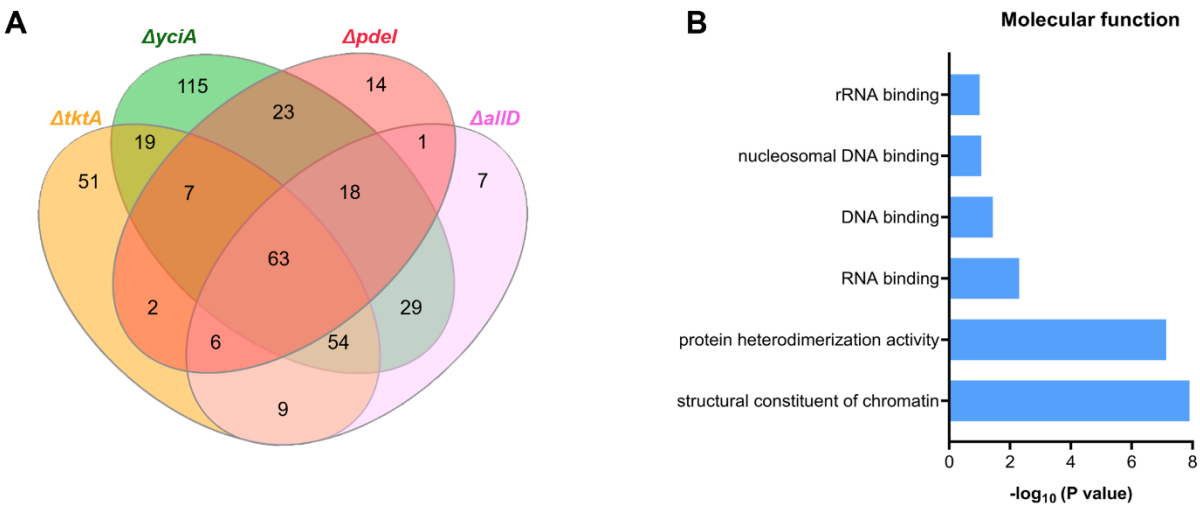

Figure S4. Different *E. coli* mutants induce similar transcriptomic changes in *C. elegans*

(A) Venn diagram showing the overlap among genes downregulated in N2 worms grown on *E. coli* mutants *ΔtktA*, *ΔyciA*, *ΔpdeI*, and *ΔallD* compared to the BW25113 control.

(B) Gene ontology enrichment analysis of molecular function for the common 63 genes downregulated in N2 worms grown on *E. coli* mutants *ΔtktA*, *ΔyciA*, *ΔpdeI*, and *ΔallD*.

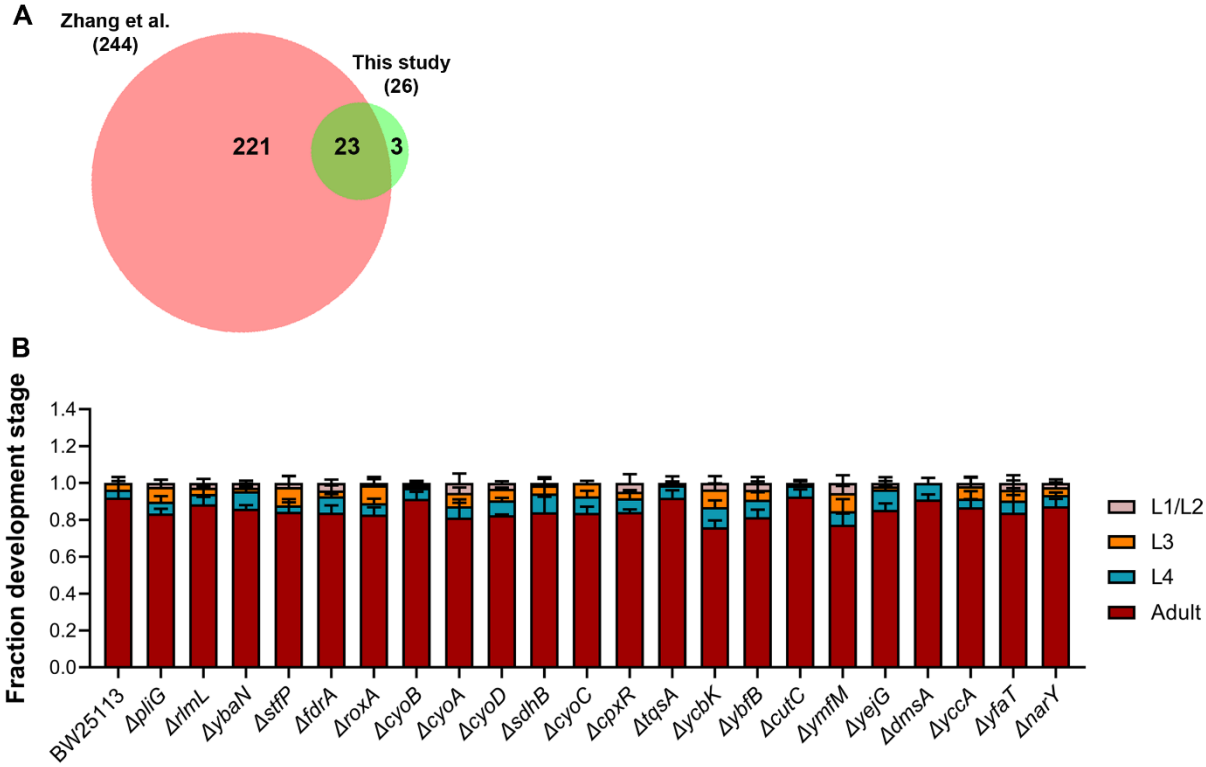

Figure S5. Iron supplementation rescues mutant diet phenotypes

(A) Venn diagram showing the overlap between *E. coli* mutants identified by (Zhang et al., 2019) and those identified in this study. The Venn diagram was obtained using the web tool BioVenn (https://www.biovenn.nl/).

(B) Quantification of different developmental stages of N2 worms grown at 20°C for 60 hours after transferring synchronized L1 larvae onto *E. coli* BW25113 and mutant diets supplemented with 4 mM ferric chloride (n = 3 biological replicates; animals per condition per replicate >60).

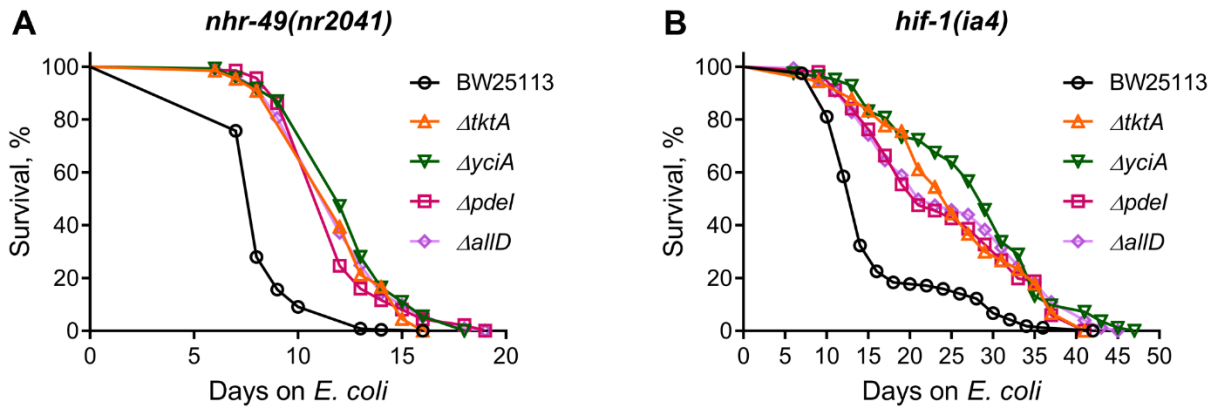

Figure S6. HIF-1 and NHR-49 are not required for lifespan extension on mutant diets

(A) Representative survival curves of *nhr-49(nr2041)* worms fed on *ΔtktA*, *ΔyciA*, *ΔpdeI*, and *ΔallD E. coli* mutants along with the BW25113 control. $p < 0.001$ for all the mutant diets compared to the BW25113 control (n = 3 biological replicates; animals per condition per replicate > 60).

(B) Representative survival curves of *hif-1(ia4)* worms fed on *ΔtktA*, *ΔyciA*, *ΔpdeI*, and *ΔallD E. coli* mutants along with the BW25113 control. $p < 0.001$ for all the mutant diets compared to the BW25113 control (n = 3 biological replicates; animals per condition per replicate > 80).

Supplementary Table

Table S1. List of *E. coli* mutants that suppress *C. elegans* FAT-7 expression

Table S2. Genes upregulated in N2 worms grown on *E. coli* mutants *ΔtktA*, *ΔyciA*, *ΔpdeI*, and *ΔallD* compared to those grown on *E. coli* BW25113

Table S3. Genes downregulated in N2 worms grown on *E. coli* mutants *ΔtktA*, *ΔyciA*, *ΔpdeI*, and *ΔallD* compared to those grown on *E. coli* BW25113